

Union College

Union | Digital Works

Honors Theses

Student Work

5-2022

Characterization of the Initial Explosive Phases of the 2021 Eruption at La Soufriere, St. Vincent

Sydney Walters

Union College - Schenectady, NY

Follow this and additional works at: <https://digitalworks.union.edu/theses>



Part of the [Volcanology Commons](#)

Recommended Citation

Walters, Sydney, "Characterization of the Initial Explosive Phases of the 2021 Eruption at La Soufriere, St. Vincent" (2022). *Honors Theses*. 2588.

<https://digitalworks.union.edu/theses/2588>

This Open Access is brought to you for free and open access by the Student Work at Union | Digital Works. It has been accepted for inclusion in Honors Theses by an authorized administrator of Union | Digital Works. For more information, please contact digitalworks@union.edu.

Characterization of the Initial Explosive Phases of the 2021 Eruption at La Soufriere, St.

Vincent

by
Sydney Walters

Submitted in partial fulfillment of the requirements for the degree of Bachelor of
Science in the Department of Geosciences

Union College

June 2022

Abstract

The Soufriere Volcano on St. Vincent Island, in the Lesser Antilles volcanic arc, is one of the most active subaerial volcanos in the Caribbean, erupting both explosively and effusively at least 7 times in the last 500 years. In December of 2020, the volcano began erupting effusively, showing no evidence of degassing and on April 9th of 2021, it transitioned to an explosive eruption that continued until April 22, with more than 30 eruptions classified as Vulcanian and sub-Plinian. Scoria samples from three units (U1-U3) erupted in the first 48-72 hours of the explosive eruptive phase were analyzed in order to determine any petrologic differences and similarities that would give insights into what triggered the transition in eruptive style and whether the explosive eruption changed as it progressed. The scoria was classified as basaltic andesite (52.8-54.2 wt% SiO₂), similar to the compositions of scoria from previous eruptions at the volcano, with a common mineral assemblage of plagioclase + orthopyroxene + clinopyroxene + olivine + titanomagnetite. Crystal sizes range from microlites (<10 µm) to >1mm phenocrysts. Phenocrysts in all samples from U1, U2, and U3 are in textural equilibrium, however they are in chemical disequilibrium with the groundmass glass. Plagioclase is either unzoned (An₅₆₋₉₆) or displays normal zoning with calcic cores (An₈₀₋₉₅) and thick (20-50µm) sodic rims (An₅₈₋₆₅). Plagioclase microlites compositions in U3 are more sodic than the phenocryst rims- suggestive of different crystallization depths. Pyroxene phenocrysts are unzoned (Mg# 0.84-0.58) and microlites are more Fe-rich, with opx more abundant than cpx in U3, whereas their frequency is approximately equal in U1 and U2. Olivine is present in all samples as unzoned phenocrysts (Fo₅₉₋₈₇) or zoned phenocrysts with thin (~5 µm) Fo₆₅ rims. Olivine microlites are abundant in U1 and U2 and are rare in U3. One distinction between the units is the vesicle size, which appears to become progressively larger over the course of the eruptive sequence,

providing evidence of over-pressurization preceding the initial explosive eruption. The lack of reversely zoned phenocrysts suggests that a mafic injection did not trigger the explosive eruption. However, based on the broad range of microlite compositions, which become more sodic during the eruptive sequence, mineral cores that are not in equilibrium with the melt, and the two populations of microlites, there is evidence for cryptic magma mingling that occurred rapidly upon ascent as a slightly more mafic melt rose into the less mafic and pre-existing magma chamber.

Acknowledgements

My most sincere thanks to Professor Holli Frey for giving me this opportunity to take part in cutting edge research, as well as for supporting me throughout my time at Union College. Holli has been such an incredible mentor for me in the Geosciences Department and has made my whole Union experience so much more special than I had ever imagined. Thank you for being my “Union College mom” and for supporting me in my academics, but most of all, for caring for me as a whole person and not just as a student. You have inspired me in so many ways and while I could write about a million other ways you have impacted my life, I just want you to know that I am eternally grateful to know you and to have built this friendship.

I would like to thank Matt Manon for his help throughout our research process, by collecting data and ensuring that the SEM was working daily, even though there was never a day without some sort of problem with the SEM (or carbon coating machine.) I also want to thank you for supporting me as my academic advisor and helping me to get the most out of my Union education. I would not be here without your support and confidence in me.

In addition, thank you to our international collaborators on this research project, Thomas Christopher at the UWI-SRC for sending scoria samples and carrying out the vesicle size distribution analyses, as well as Jenni Barclay, from the University of East Anglia, and Paul Cole, from the University of Plymouth, for collecting samples and collaborating on analyses. I am also extremely grateful to have had the support and funding from the Union College Undergraduate Research Committee and the National Science Foundation (NSF), both of whom have supported this cutting edge research through funding so that we may help to keep people safe in the case of future volcanic eruptions.

Finally, many thanks go out to my friends and family for their ongoing support and guidance throughout my education. A special thank you goes out to my parents and my sister for always listening to me as I would try to explain my research and new-found knowledge throughout the research process, even though they understand none of what I was talking about. Without your support and unconditional love, I would not be the woman and scientist I am today.

Table of Contents

Abstract	i
Acknowledgements	iii
Introduction	1
<i>Effusive and explosive eruption transition s.</i>	1
<i>Geologic setting and research location</i>	2
<i>The Island of St. Vincent and La Soufriere Volcano.</i>	4
<i>Previous eruptions</i>	4
<i>Current transitional eruption</i>	7
<i>This study</i>	7
Sampling and analytical methodology	13
<i>Origin and characterization of samples</i>	13
<i>Geochemical analysis</i>	15
<i>Textural analysis</i>	15
<i>Crystal composition analysis</i>	16
<i>Vesicle size distribution</i>	16
Results	17
<i>Bulk whole rock chemistry</i>	17
<i>Petrography</i>	17
<i>Mineral phases</i>	18
<i>Plagioclase – phenocrysts.</i>	18
<i>Plagioclase – microlites</i>	19
<i>Plagioclase – FeO content and glomerocrysts</i>	28

<i>Olivine – phenocrysts</i>	32
<i>Olivine – microlites</i>	33
<i>Olivine – glomerocrysts</i>	33
<i>Clinopyroxene (Cpx) – phenocrysts</i>	39
<i>Clinopyroxene (Cpx) – microlites</i>	40
<i>Clinopyroxene (Cpx) – glomerocrysts</i>	40
<i>Orthopyroxene (Opx) – phenocrysts</i>	46
<i>Orthopyroxene (Opx) – microlites</i>	47
<i>Orthopyroxene (Opx) – glomerocrysts</i>	47
<i>Titanomagnetite</i>	54
<i>Dome Fragments and Xenocrysts</i>	57
<i>Vesicle size distribution</i>	58
<i>Gas and hydrothermal monitoring</i>	60
Discussion	62
<i>Origin of Soufriere magmas – comparison of current magma to prior magmas</i>	62
<i>Crystal textures and introduction of magma from depth</i>	64
<i>Closed to open system transition – hydrothermal gas analysis</i>	68
<i>Closed to open system transition – vesicle nucleation and coalescence</i>	68
Conclusion	70
References	72

Table of Contents – Figures

Figure 1. Geographic map of Lesser Antilles arc and island of St. Vincent	3
Figure 2. Timeline of St. Vincent’s eruptive history	6
Figure 3. Satellite image of lava dome growth	9
Figure 4. Map of volcanic centers on St. Vincent	14
Figure 5. Cross section of volcanic debris	15
Figure 6. TAS diagram	17
Figure 7. BSE image of U1 plagioclase	20
Figure 8. Histogram of U1 plagioclase compositions	21
Figure 9. BSE image of U2 plagioclase	22
Figure 10. Histogram of U2 plagioclase compositions	23
Figure 11. BSE image of U3 plagioclase	24
Figure 12. Histogram of U3 plagioclase compositions	25
Figure 13. BSE image of plagioclase microlites	26
Figure 14. Pie chart of U1 zoned and un-zoned plagioclase microlites	27
Figure 15. Pie chart of U2 zoned and un-zoned plagioclase microlites	27
Figure 16. Pie chart of U3 zoned and un-zoned plagioclase microlites	28
Figure 17. Scatter plot of FeO compared to An mol%	29
Figure 18. Scatter plot of FeO content in U1 phenocrysts versus glomerocrysts	30
Figure 19. Scatter plot of FeO content in U2 phenocrysts versus glomerocrysts	31
Figure 20. Scatter plot of FeO content in U3 phenocrysts versus glomerocrysts	32
Figure 21. BSE image of U1 olivine	34
Figure 22. Histogram of U1 olivine compositions	35

Figure 23. BSE image of U2 olivine	36
Figure 24. Histogram of U2 olivine compositions	37
Figure 25. BSE image of U3 olivine	38
Figure 26. Histogram of U3 olivine compositions	39
Figure 27. BSE image of U1 clinopyroxene	41
Figure 28. Histogram of U1 clinopyroxene compositions	42
Figure 29. BSE image of U2 clinopyroxene	43
Figure 30. Histogram of U2 clinopyroxene compositions	44
Figure 31. BSE image of U3 clinopyroxene	45
Figure 32. Histogram of U3 clinopyroxene compositions	46
Figure 33. BSE image of U1 orthopyroxene	48
Figure 34. Histogram of U1 orthopyroxene compositions	49
Figure 35. BSE image of U2 orthopyroxene	50
Figure 36. Histogram of U2 orthopyroxene compositions	51
Figure 37. BSE image of U3 orthopyroxene	52
Figure 38. Histogram of U3 orthopyroxene compositions	53
Figure 39. BSE image of orthopyroxene microlites	54
Figure 40. BSE image of U1 titanomagnetite	55
Figure 41. BSE image of U2 titanomagnetite	56
Figure 42. BSE image of U3 titanomagnetite	57
Figure 43. BSE image of a xenocryst	58
Figure 44. BSE image of the vesicle size distribution in U1	59
Figure 45. BSE image of the vesicle size distribution in U2	59

Figure 46. BSE image of the vesicle size distribution in U3	59
Figure 47. Chart of hydrothermal element signatures in water samples	61
Figure 48. BSE image of a xenocryst	63
Figure 49. BSE image of xenocryst compositions (zoomed in view of figure 48)	64

Introduction

Subduction zone volcanism is one of the most exciting yet terrifying processes that occurs on Earth, producing large explosions of silica rich magma, large scale earthquakes, ash plumes that fill the sky, and pyroclastic flows that roll down the flanks of the volcano, decimating everything in their paths with a mix of hot gasses and ash. Subduction zones produce stratovolcanoes, which are formed by viscous lava that sticks to slopes of the volcano, building up around its vent. Stratovolcanoes erupt in multiple ways, including both effusive and explosive eruption manners, however they can also alternate between both manners throughout the same eruptive period, which can be extremely dangerous. When erupting effusively, a lava dome tends to build up and is composed of silicic and viscous lava that extrudes from fissures at a slow rate. However, when erupting explosively, large plumes of ash and scoria are erupted into the atmosphere and are followed by pyroclastic flows that sweep down the flanks of the volcano at speeds of up to 100 mph and over 1000 °C.

Effusive and explosive eruption transitions

Around the world, there are stratovolcanoes that fluctuate between effusive and explosive eruption styles in which they begin with a series of multiple explosions of scoria and ash, followed by a sustained period of controlled dome building activity within the crater (e.g. Mount Saint Helens). They can also begin by erupting effusively and then quickly transitioning into an explosive eruption within a matter of hours (e.g. Soufriere Hills, Montserrat). Eruptive styles can be determined by external processes and influences as they are more available to record and study, but effusive and explosive transitions can also be triggered by internal processes. An example of this eruption style transition that has been thoroughly studied is at the Methana

volcano, located in the Aegean Sea, which has a long history of effusive to explosive eruption transitions.

When studying Methana and analyzing what causes the volcano to transition between eruptive styles, Popa et. al., (2020) found that it is often the internal processes taking place within the conduit that are likely to provide evidence for changes within the magma chamber. Based on analyses of previously erupted scoria, as well as effusive dome clasts, evidence was found that gave insight into what may occur at certain depths within the magmatic system that leads to effusive and explosive eruptions. The Methana volcanic system showed that based on equilibrium calculations of phenocryst compositions, zoning patterns, and groundmass glass compositions, different types of magmatic end-member interactions are going to produce different types of eruptions. For example, the mixing of upper-crustal silicic magmas (evolved) with more mafic (recharge) magmas, basaltic andesites, is likely to produce more effusive style eruptions with scoria compositions being more biased by the mafic recharge component. However, the mixing of low inputs of upper-crustal silicic magmas with more evolved mafic recharge magmas are likely to produce explosive eruptions (Popa et. al., 2020).

Geologic setting and research location

Effusive to explosive eruption transitions are also extremely common in the Caribbean Sea at one of the most active volcanic areas today, the Lesser Antilles, which is a 750 km-long intra-oceanic island arc that is located in the Caribbean Sea, just north of Venezuela (Fig. 1). The island arc is created due to the slow subduction (~2-4 cm per year) of the North Atlantic plate under the Caribbean plate, creating an active volcanic arc that is home to some of the most active subaerial volcanoes in the world (Fedele et. al., 2021). Among these volcanoes is La Soufriere,

on the island of Saint Vincent, just south of Saint Lucia, which has a long history of active volcanism, dating back to prehistoric times (Fig. 1). As St. Vincent is located at the southern end of the arc (St. Vincent to Grenada, north to south), it is considered to be one of the juvenile products of the Lesser Antilles arc, which means that it is erupting predominantly less evolved magmas (basalts to andesites). The northern and central sections of the arc (St. Lucia to Saba, south to north) erupt more evolved magmas, such as andesites, dacites, and rare rhyolites (Fedele et. al., 2021).

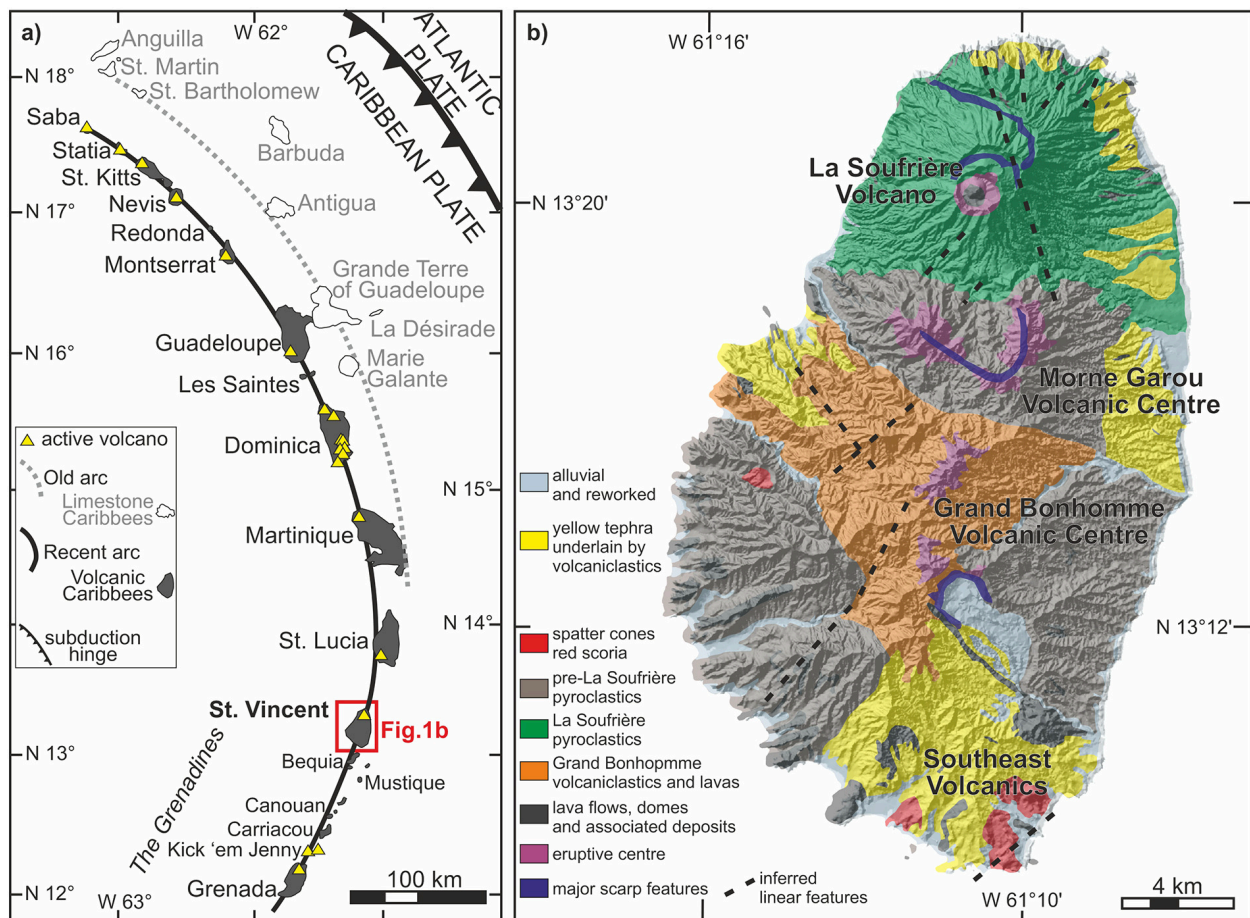


Figure 1. Left: a geographic map of the Lesser Antilles island arc and its location relative to the Atlantic-Caribbean subduction zone. St. Vincent, where this study takes place, is outlined by the red square. Right: a map of the island of St. Vincent in which the different volcanic centers are indicated by different colors (taken from Fedele et. al., 2021).

The Island of St. Vincent and La Soufriere Volcano

La Soufriere is a 1,204 meter stratovolcano, dominating the northern half of the island of St. Vincent. La Soufriere is one of the most active subaerial volcanic centers in the Caribbean, having recorded at least 8 separate eruptive periods in the last 500 years (Fig. 1). In the last century alone, La Soufriere has erupted in four separate periods, 1902-03, 1971-72, 1979, and most recently in December 2020 – April 2021. While all eruptions have been confirmed based on radiocarbon dating of charcoal found within volcanic deposits on the island, the 1971-72 lava dome, 1979 eruption, and 1902-03 eruptions have been thoroughly studied both petrologically and from historical accounts in order to determine causation for the multiple explosions (Cole et. al, 2019).

Previous Eruptions

La Soufriere does not always erupt in the same manner as it has documented eruptions that have been exclusively effusive or explosive, as well as a combination of the two. The 1902-03 series of explosive eruptions had an extreme impact on the island of St. Vincent, producing large ash plumes and fallout over the many populated towns around the volcano, which resulted in more than 1500 fatalities and extensive damage to infrastructure. Throughout the one year duration of eruptivity, which was preceded by increasing numbers of earthquakes, rockfalls, landslides, there were three main periods of explosivity, the first beginning on May 7th as the largest phreatomagmatic explosion due to the crater being filled with water (Pyle et. al, 2018). The second period of eruptions, occurring from September to October, were smaller in scale and contained no hydrous component like the first (Fig. 2). The final period of explosivity took place in March of 1903 before the volcano went back into a resting state. Basaltic andesite scoria

samples from the different periods of the 1902-03 eruptions were analyzed later in order to determine the internal trigger for the explosive eruptions (Heath et. al., 1998a). Evidence was found in the reversely zoned textures of the plagioclase phenocrysts in the scoria thin sections, as well as in the whole rock composition analyses, which determined that there were both basaltic andesite and basaltic samples (Fedele et. al., 2021). The reverse zoning of the plagioclase, as well as the basaltic scoria clasts were indicative of a mafic injection in which a hotter and more mafic magma body was injected into La Soufriere's main magma chamber. The mixing of the hotter magma body with La Soufriere's main magma body created disequilibrium within the volcano and the build-up of volatiles that over-pressurized system, resulting in the explosive eruption style (Fedele et. al., 2021).

La Soufriere began erupting effusively in November of 1971 as a lava dome formed over the course of approximately 5 months (Fig. 2). The effusive activity occurred as a lava dome accumulated within the crater of the volcano, which was filled by a crater lake. This eruptive period remained effusive, never transitioning to an explosive eruptive style and the lake held within the crater remained until the initial explosive eruption in 1979 (Fournier et. al., 2011). According to Fournier et. al. (2011), the crater lake was filled with fresh water and freshwater sediments, like organic clays, which likely mixed with hydrothermal fluids below the crater, resulting in intermingling of fluids that produced disequilibrium and subsequently the explosive nature of the eruption.

Prior to the most recent eruption that this study will focus on, La Soufriere last sustained eruptive activity in 1979, beginning in April and ending in late October (Fig. 2). Eruptive activity began with a large phreatomagmatic explosion, reaching approximately 18km above sea level, followed by series of Vulcanian style eruptions (Cole et. al, 2019). The explosive eruptions were

short lived, as the final one occurred in early May and was followed by a long period of effusivity that created the lava dome that filled the crater until activity ended in late October of 1979. Samples from the eruption's scoria blocks and pyroclastic flow units were sampled in 1981 and were classified as basaltic andesite with a common mineral assemblage of plagioclase, clinopyroxene, orthopyroxene, olivine, and titanomagnetite (Graham and Thirlwall, 1981). Phenocryst textures showed mostly euhedral edges with some dendritic growth that was likely due to super-cooling from the incorporation of liquid of rapidly growing crystal surfaces. Additionally, clinopyroxene phenocrysts had highly magnesium-rich cores, which suggested the possibility of some of the magma coming from a more mafic, or primitive, source (Graham and Thirlwall, 1981).

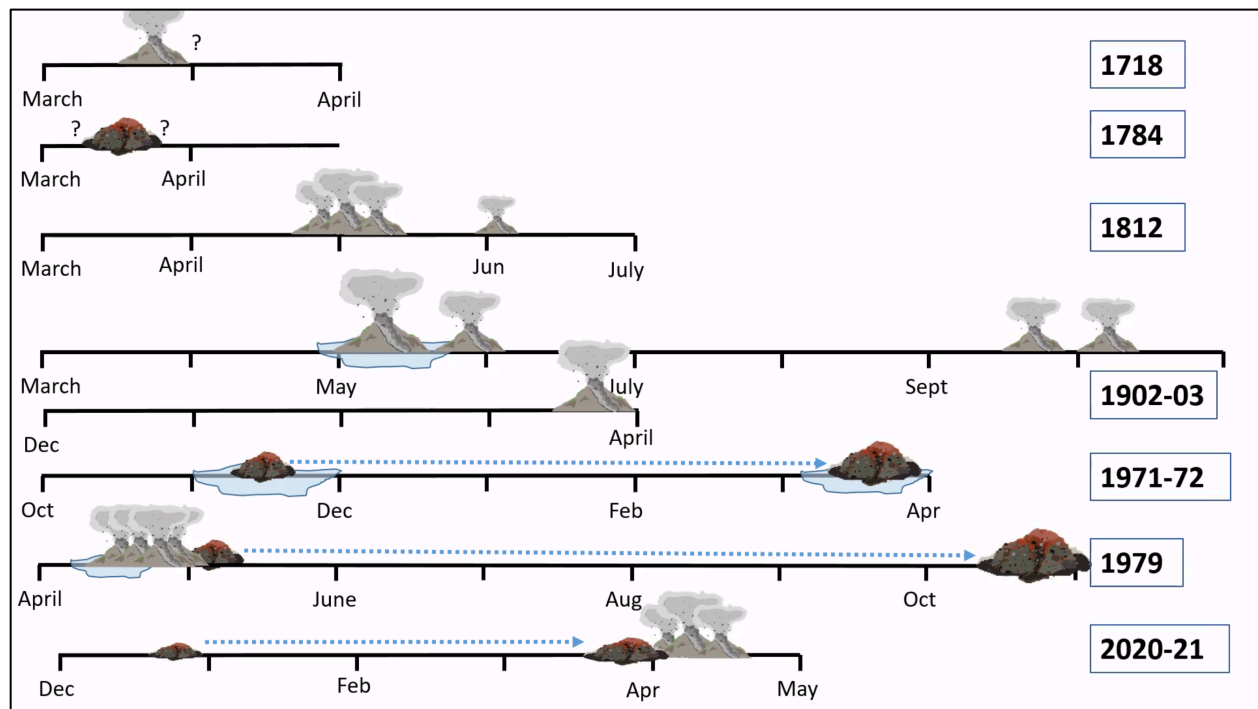


Figure 2. A timeline of St. Vincent's active volcanic history over the last 500 years that includes the 6 documented eruptions, as well as the most recent eruption in 2021 (Image from Barclay, pers. comm.).

Current transitional eruption

The La Soufriere volcano began erupting effusively in late December of 2020, creating a lava dome along the western base of the pre-existing 1979 lava dome. The dome building activity continued over the course of approximately 3 months in which it grew to fill the rest of the space within the crater that was not taken by the 1979 dome (Fig. 2 and 3). The volcano transitioned to an explosive eruption style on April 9, 2021, and over the course of the following two weeks, there were more than 30 separate Vulcanian and sub-Plinian explosions that occurred in which the ash plume rose 8-16km in height; explosive activity ceased on April 22, 2021 (UWI-SRC FAQ). Pyroclastic flows were a result as the ash from the eruption plumes began to fall intermittently throughout explosive activity and lahars decimated towns and villages due to the mixing of the accumulated ash and incoming rain from hurricanes. Volcanic monitoring was performed by the University of the West Indies Seismic Research Centre (UWI-SRC) for the duration of the 2021 eruption, from December to the present, allowing for volcanologists to monitor seismic activity below the island, deformation within the crater and around the flanks of the volcano, and water samples. Due to the immense monitoring being performed by the UWI-SRC, the island's 16,000 person population was evacuated approximately 12 hours prior to the initial explosion and thus, there were zero casualties.

This study

In order to understand what may have triggered the transition from an effusive to explosive eruption style, it is important that we look for evidence of both external and internal triggers. Based on monitoring data that was collected by the UWI-SRC between the start of effusivity in late December until early April, no evidence has been found for an external

influence on the eruptive style. Therefore, it is crucial to study scoria clasts that were erupted at the beginning of explosivity in order to determine if there are internal influences from the magmatic system. Similar to how the Methana volcano was studied by Popa et. al. (2020), we will look into multiple different aspects of the scoria samples, including bulk whole rock chemistry, phenocryst and microlite compositions, textures, and zoning patterns, as well as vesicle size distribution during the initial explosive phases.

Bulk whole rock chemistry is important to understand when studying scoria clasts as it allows for the classification of the type of lava being erupted based on the overall silica content. Since different volcano types and locations produce different product compositions, the composition of the whole rock from the La Soufriere eruption in 2021 can be compared to historical eruption products in order to see if the magmatic source within the volcano has changed between periods of eruption.

Phenocryst analysis is crucial in understanding the pressure and temperature conditions within the magmatic system, as different minerals are stable at different conditions. Once the common mineral assemblage in the scoria clasts has been classified, we can study the textures of the phenocrysts and look for signs of disequilibrium that would tell us if the crystals are growing within the melt or if they are forming in different pressure (P) and temperature (T) conditions. Thus, we will be looking for textures like coronas, dissolution, embayments, and sieve textures that will suggest different P/T conditions where they initially grew.

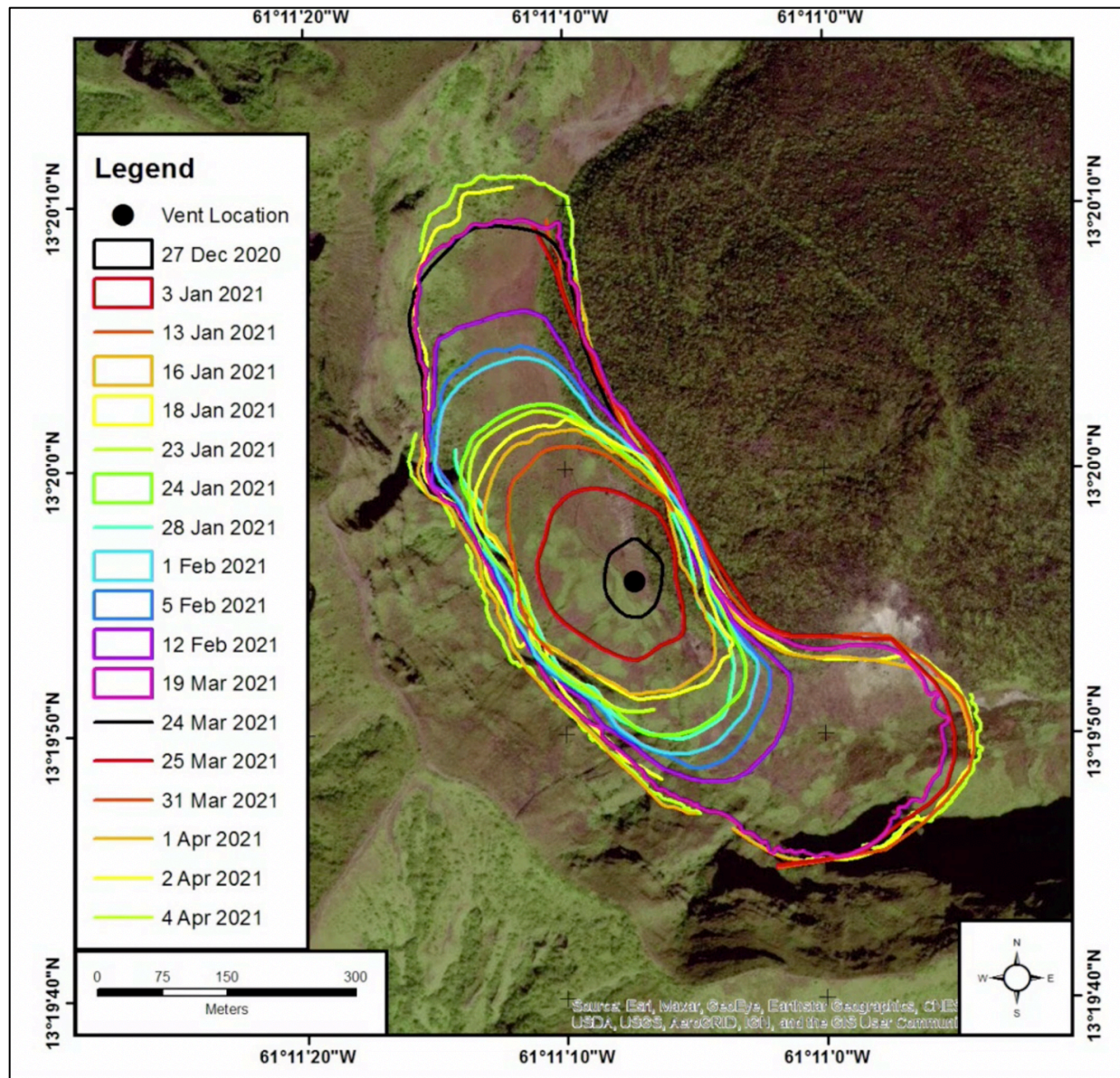


Figure 3. A satellite image of the progression of growth of the 2021-2022 lava dome that formed in the crater of La Soufriere, alongside the 1979 lava dome (UWI-SRC Scientific Advisory Report April 4, 2021)

Compositional differences between the products of effusive versus explosive eruptions are often difficult to identify when trying to understand the internal influences on eruption style, as the whole rock chemistry represents a mixture of two different magmas. However, textural and compositional differences of specific crystals within the scoria can be analyzed to gain a better understanding of what types of magmas may be mixing. Thus, it is crucial to study

phenocryst chemical compositions, microlite chemical compositions, textural differences, and zoning patterns in order to find evidence of different P/T conditions, volatile content, and magma sources.

As phenocrysts are the most dominant feature when analyzing scoria under a microscope, it is important to understand the chemical compositions of each mineral phase in order to characterize the common mineral assemblage, which also helps to define the main magma body chamber. Different mineral assemblages are stable at certain pressure and temperature conditions, which result in different amounts of silica being included in scoria. For example, a common scoria type for subduction zone volcanoes, specifically La Soufriere, is a basaltic andesite, which has a common mineral assemblage of plagioclase, clinopyroxene, orthopyroxene, olivine, and titanomagnetites. Along with the characterization of mineral compositions, crystal textures provide evidence of the state of equilibrium of the magma prior to eruption.

While phenocrysts are the first feature to stand out when looking at scoria under a microscope, more information can be extracted from microlites that are found in the melt. Microlites are smaller crystals ($<100\text{ }\mu\text{m}$), and they give insight into changes within the magmatic system over very short periods of time. Microlites form upon magma ascent in the conduit and thus, provide information about how fast the magma is rising, how the pressure and temperature conditions are changing within the conduit, as well as how long the magma is spending time at certain depths upon ascent. For example, Preece et. al. (2013) studied groundmass microlites from the 2006 effusive to explosive eruption of Merapi volcano, in Indonesia, and found that higher ascension rates of magma resulted in a higher density of microlites within the groundmass upon eruption.

Contrastingly, slower ascension rates of magma, and subsequently lower effusion rates at the surface result in a lower microlite density in the groundmass (Preece et. al., 2013).

Equilibrium and disequilibrium textures are indicators of internal influences within the magma chamber that occur prior to eruption. When minerals are in equilibrium with the melt, that means that they are growing from the melt itself, pulling chemicals out of the melt and forming crystals through a process called crystal fractionation. Crystals that are in equilibrium will show defined and euhedral edges. When minerals are in disequilibrium with the melt, they likely did not form from the particular melt in which they are found. Instead, they would have to form in another body of magma that is from different pressure and temperature conditions where they are stable and can form euhedral edges. The crystals are then introduced into another magma body with melt, volatile, pressure, and/or temperature conditions that may be dissimilar to those that they formed in, causing the euhedral edges to undergo dissolution. Disequilibrium textures can appear in many varieties, like sieve textures, reverse zoning, dissolution, coronas, or embayments (Preece et. al., 2013).

Other textures that are extremely common in both phenocrysts and microlites are zoning patterns, which are classified as either normal or reverse, and are most often seen in plagioclase. Normal zoning patterns are often caused by decreases in water content or temperature within the magma and can be clearly seen through back scatter electron imaging, performed by a scanning electron microscope. Phenocrysts that are normally zoned will show heavier cations in lighter gray shades, and lighter cations in darker gray rims. For plagioclase, normal zoning shows Ca-rich cores and Na-rich rims whereas while olivine crystals that are normally zoned will show Mg-rich cores and Fe-rich rims. Reverse zoning shows the opposite trend in which crystals will show dark gray cores and light gray rims. Reverse zoning of plagioclase is often a tell-tale

indicator of a mafic injection as an influx of a hotter magma will change the order of fractionation within the main magma body. The 1902-03 eruption of La Soufriere showed evidence of reverse zoning of plagioclase in scoria clasts, leading scientists to conclude that the eruption was triggered by a mafic injection (Graham and Thirlwall 1981). Additionally, gas build up is one of the most important factors that results in explosive eruptions and therefore, it is crucial to look for trends in the size of vesicles in the scoria, as well as the number of vesicles present, which gives context about the rate of nucleation throughout the course of the different explosive eruptions (Preece et. al., 2013).

The goal of this study is to find evidence that will give insight into what kind of internal trigger may have caused La Soufriere to transition from an effusive to explosive eruption style so as to better understand, monitor, and predict future activity at the volcano. In order to do so, it will be crucial to first characterize what erupted explosively during the 2021 eruption and understand how it compares to historical eruptions and then use the chemical and textural evidence to determine how the magmatic system changed through dome growth and explosivity. Being able to predict effusive and explosive eruption transitions is one of the most challenging feats in the field of volcanology. However, by studying the eruptive history of the volcanic system and determining what has triggered the style of eruption in the past, scientists can better monitor active volcanoes and ultimately, keep those who live near and around volcanic centers safe.

Sampling and analytical methodology

Origin and characterization of samples

Scoria clasts from the initial three explosive phases of the La Soufriere eruption were collected from Sandy Bay (U1 and U2 samples) and Rabacca Bridge (U3 samples), which are located on the southeast flanks of the volcano (Fig. 4). Samples from U1, U2, and U3 were deposited within the first 48 hours of explosivity and are characterized by large and small scoria clasts in the first deposit (U1), ash with thin and intermittent layers of different-sized scoria clasts (U2), and intermittent layers of ash, larger scoria clasts, and pyroclastic density flow debris (U3) (Fig. 5). Sixteen clasts total were cut and turned into thin sections with two being from the first explosive unit (U1), two from the second explosive unit (U2), and twelve from the third explosive unit (U3).

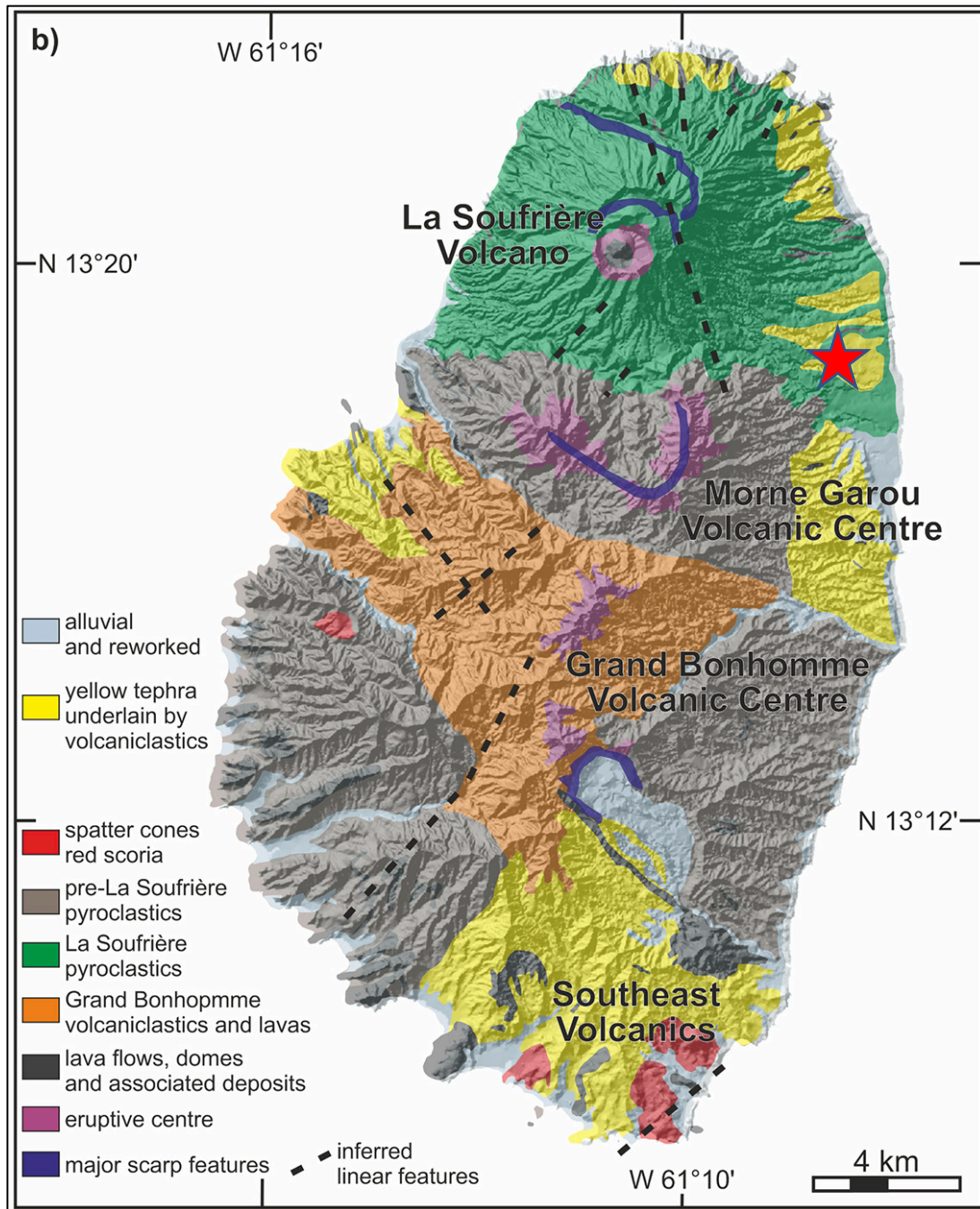


Figure 4. A map of the different volcanic centers on St. Vincent, with La Soufrière located in the north. Samples were collected on the southeast flanks of the volcano, indicated by the red star (Bouysse et al., 1990, Robertson, 2005, and Fedele, et. al., 2021).

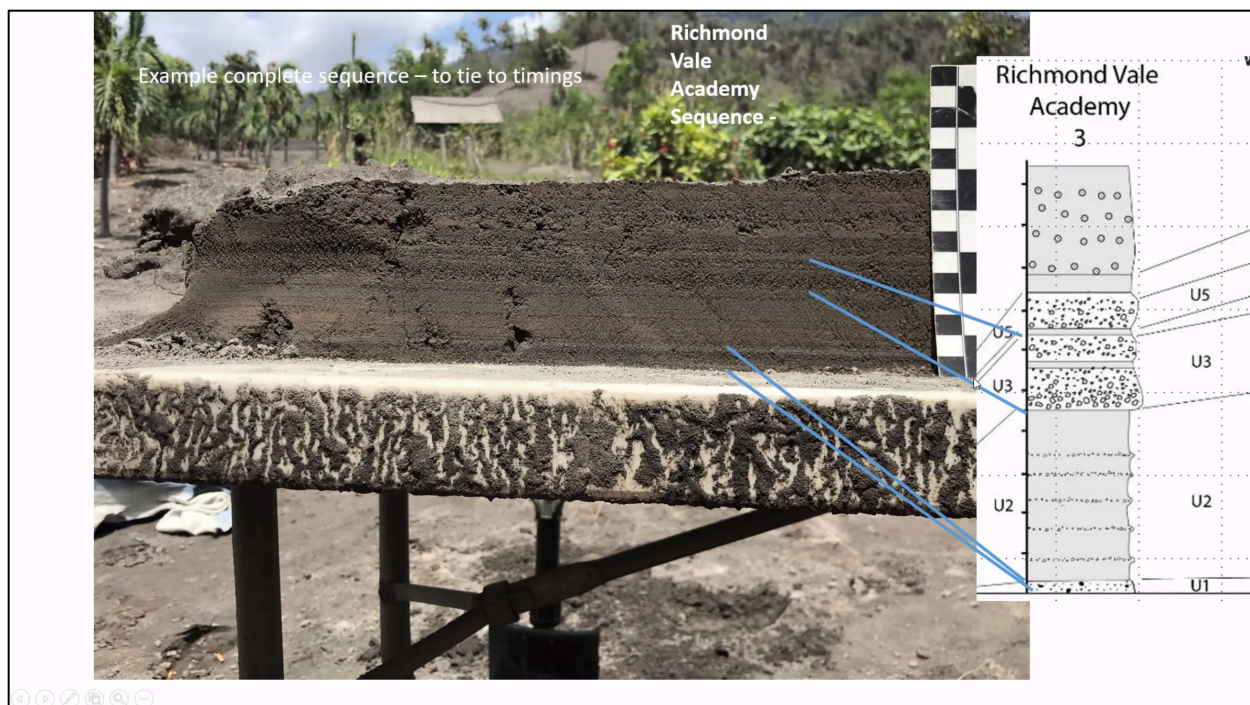


Figure 5. A cross-section of the initial layers of debris that were deposited during the explosive eruptive phase at La Soufriere.

Samples being analyzed are collected from layers U1, U2, and U3, which are depicted at the bottom of the Richmond Vale Academy sequence.

Geochemical analysis

Whole rock compositions of 2021 scoria samples were obtained through inductively coupled plasma mass spectrometry (ICP-OES) at Bureau Veritas (Vancouver, CA), which determined the silica content, all major elements, and select trace elements of the scoria clasts being analyzed.

Textural analysis

Textural analyses of 2021 scoria samples were carried out using back-scattered electron (BSE) images of carbon-coated and polished thin sections acquired with a Zeiss EVO MA15 scanning electron microscope (SEM) at Union College, using an accelerating voltage of 15kv, a beam current of 40.0 μ A, and a working distance of 8.5mm. Multiple BSE images were taken of

crystals of different compositions and size, microlite-dense groundmass, glass textures, and overall vesicle size and distribution.

Crystal composition analysis

Chemical compositions of phenocrysts and microlites were acquired using the Bruker EDS spectrometer that is attached to the SEM. Each chemical spectra was then quantified to gauge elemental abundances in each crystal. All feldspar, pyroxene and olivine spectra were quantified using “feldsparstandardless” quantification parameters while all magnetite spectra were quantified using “oxidestandardless” quantification parameters.

Additional crystal and chemical composition analyses were performed by Professor Matthew Manon at University of Massachusetts in Amherst, using an electron microprobe (Manon and Frey, 2022, unpublished).

Vesicle size distribution

Vesicle size distribution of scoria clasts from 2021 samples were analyzed and calculated by Thomas E. Christopher at the Montserrat Volcano Observatory (MVO).

Results

Bulk Whole Rock Chemistry

U3 samples were analyzed for bulk whole rock chemistry and the scoria samples are classified as a basaltic andesite (52.8-54.2 wt% SiO₂ (Fig.6). The composition of the groundmass is andesite-dacite (62-64 wt% SiO₂).

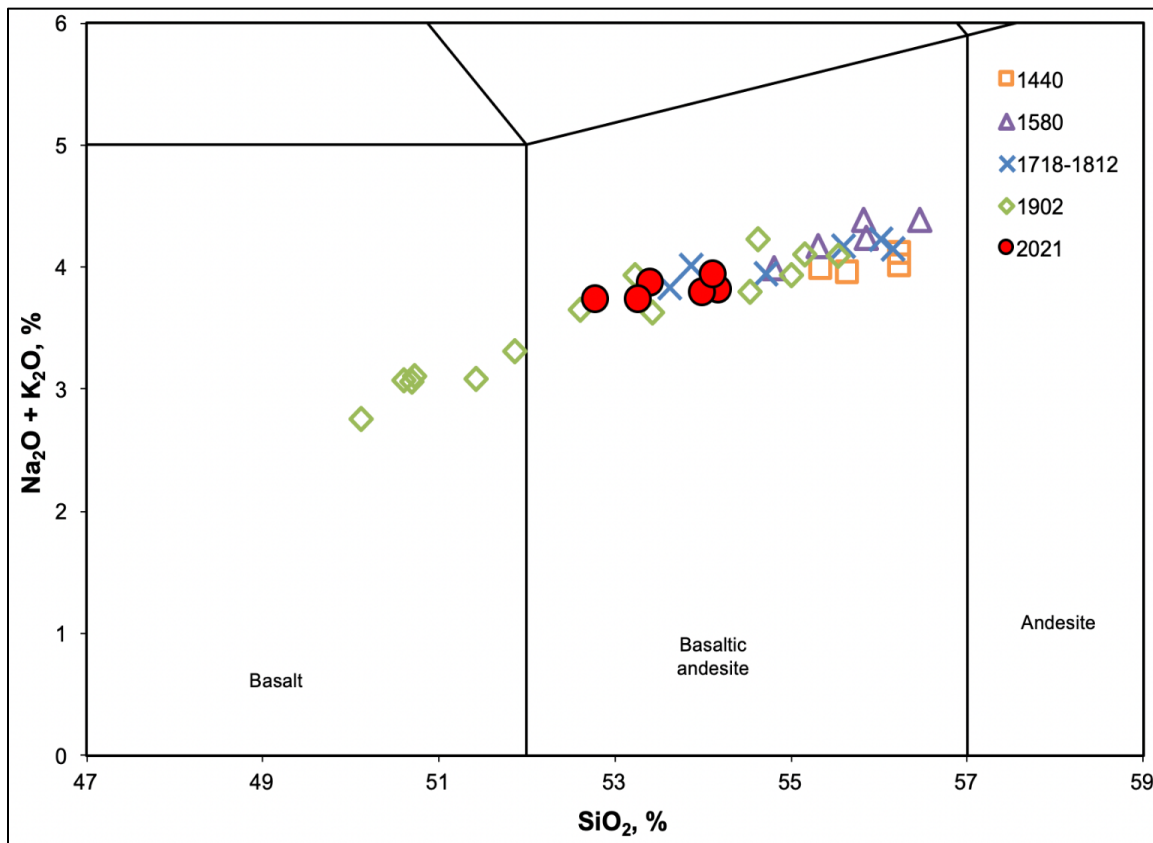


Figure 6. The TAS (total alkali vs silica) diagram that classifies the bulk whole rock chemistry of the scoria as basaltic andesite in composition. Sample analyses from the 2021 eruption have been plotted along with samples from historic eruptions at La Soufriere in order to show how the composition of what was most recently erupted compares to compositions of previous eruptions (Fedele et. al., 2021).

Petrography

Scoria samples share a common mineral assemblage of plagioclase + orthopyroxene + clinopyroxene + olivine + titanomagnetite, which is typical of the historic eruptions for La

Soufrière (Fedele et. al., 2021). Mineral phases range in size from microlites ($<100\mu\text{m}$ to $>1\text{mm}$) phenocrysts and appear as isolated phenocrysts or glomerocrysts with multiple phases.

Xenocrystic fragments are present in few scoria samples from different eruptive units, showing disequilibrium textures (dissolution) and mineral compositions representative of hydrothermal alteration during dome building events (pyrite, albite, hematite).

Mineral Phases

Plagioclase- phenocrysts

Plagioclase crystals occur in all samples from the first (U1), second (U2), and third (U3) explosive units as microlites (smaller than $50\mu\text{m}$) to phenocrysts that are larger than 1mm in diameter. Plagioclase phenocrysts in U1 appear as isolated and euhedral or shattered due to the force of the eruption, but there is no evidence of disequilibrium textures, such as coronas, embayments, or sieve textures (**Fig. 7**). Phenocrysts occur both un-zoned and normally zoned in all samples while un-zoned phenocrysts are most common. Un-zoned phenocrysts span a range of compositions (An_{60-95}) with a broad peak of An_{75-95} . Normally zoned phenocrysts show calcic cores with thick ($20-50\mu\text{m}$) sodic rims. Core compositions peak at An_{75-95} and rim compositions peak at (An_{58-65}) (Fig. 8). Phenocrysts in U2 show the same euhedral shape and textures, as well as appearing both un-zoned and normally zoned (Fig. 9). Un-zoned phenocrysts and normally zoned cores are largely calcic (An_{75-95}) while normally zoned rims remain largely sodic (An_{55-65}), similar to crystals studied in U1 (Fig. 10). More than half of the plagioclase phenocrysts in U3 samples feature distinct normal zoning, with calcic cores and thick sodic rims (Fig. 11). Un-zoned phenocrysts compositions range from An_{56-96} with a peak around An_{80-95} . Normally zoned cores are largely calcic (An_{80-95}) while rims are largely sodic (An_{58-65}) (Fig. 12).

Plagioclase- microlites

Plagioclase microlites occur in all samples from U1, U2, and U3 as a range of sizes from $<2\mu\text{m}$ to $100\mu\text{m}$ (Fig. 13). Microlite compositions in U1 cover a broad range of An_{60-95} , with most samples falling within an anorthite composition of An_{75-95} , and a significant number are more calcic than phenocryst rims (Fig. 8). Microlites in U2 not as calcic as in U1, having compositions of An_{70-85} and a peak at An_{75-80} (Fig. 10). Microlites in U3 are generally more sodic (An_{45-65}) than microlites in U1 and U2, as well as the phenocryst rims (An_{60-70}) in all units. In addition, there appear to be two separate populations of microlites, one of which is normally zoned and the other being Na-rich and un-zoned (Fig. 13). Microlites appear in all three eruptive phases as both un-zoned and normally zoned (Fig. 8, 10, and 12). Zoned microlites are most abundant in U1, but progressively decrease in number through the eruptive sequence to U3 (Figs. 14, 15, 16). The un-zoned microlites have An compositions that range An_{45-70} and the normally zoned microlites have calcic cores that have a compositional range that goes up to An_{95} , however the rims of these microlites remain similar in composition to the un-zoned microlites.

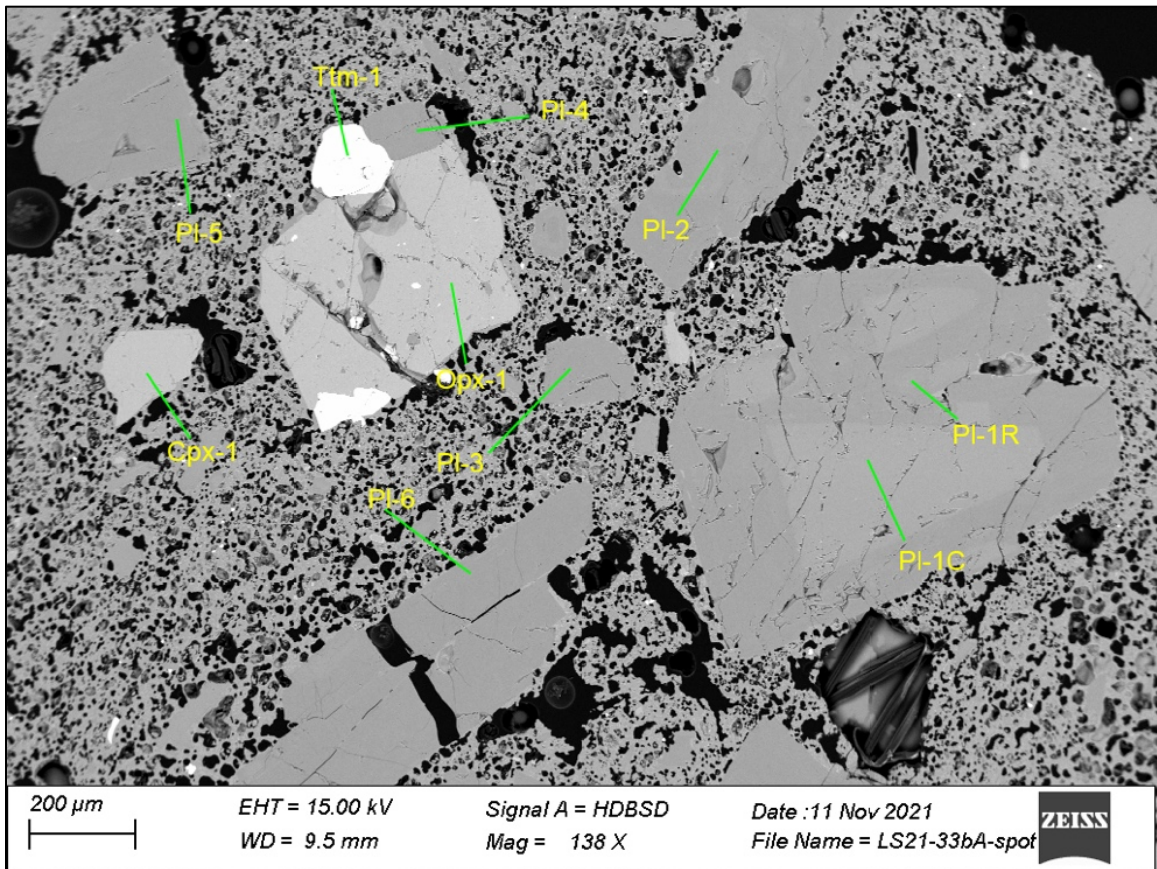


Figure 7. A BSE image from U1 showing that plagioclase crystals are typically euhedral, with some shattered by the force of the eruption.

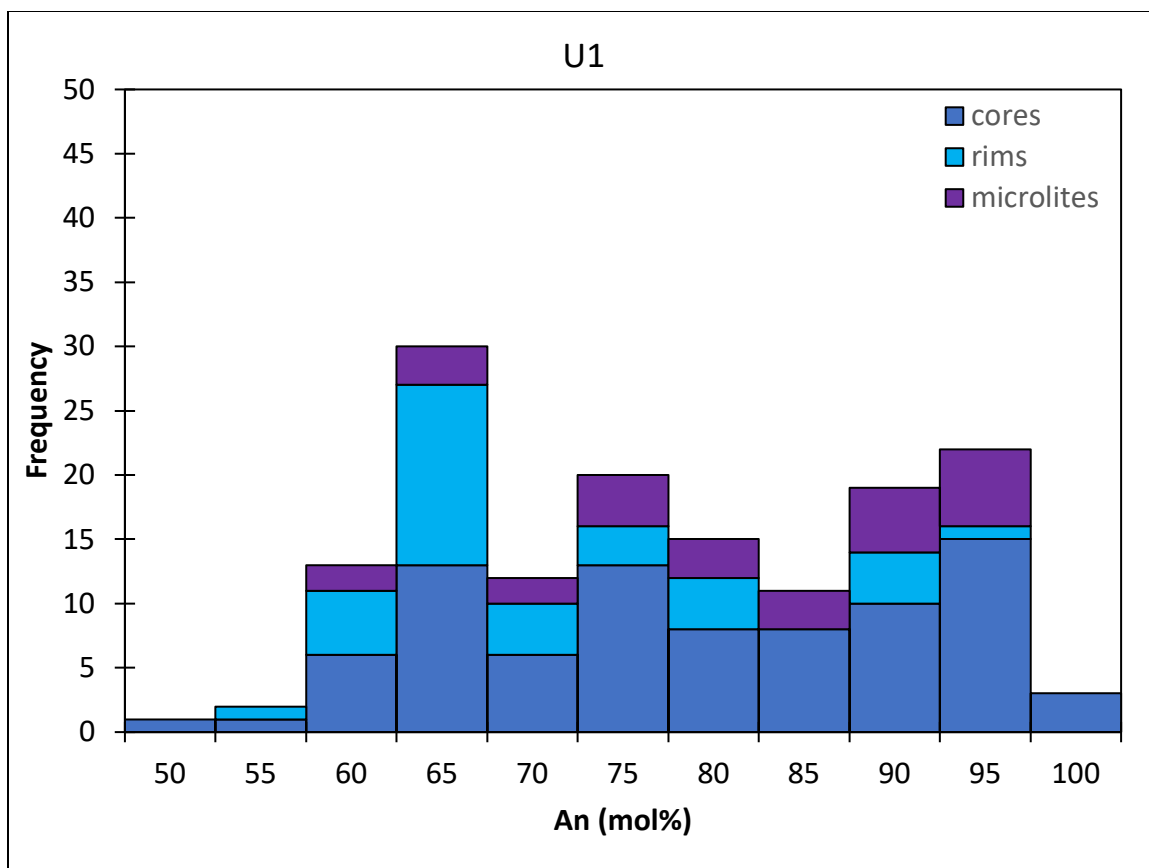


Figure 8. A histogram of plagioclase in U1 that is plotting number of plagioclase cores, normally zoned rims, and microlites within bins of 5 mol% anorthite.

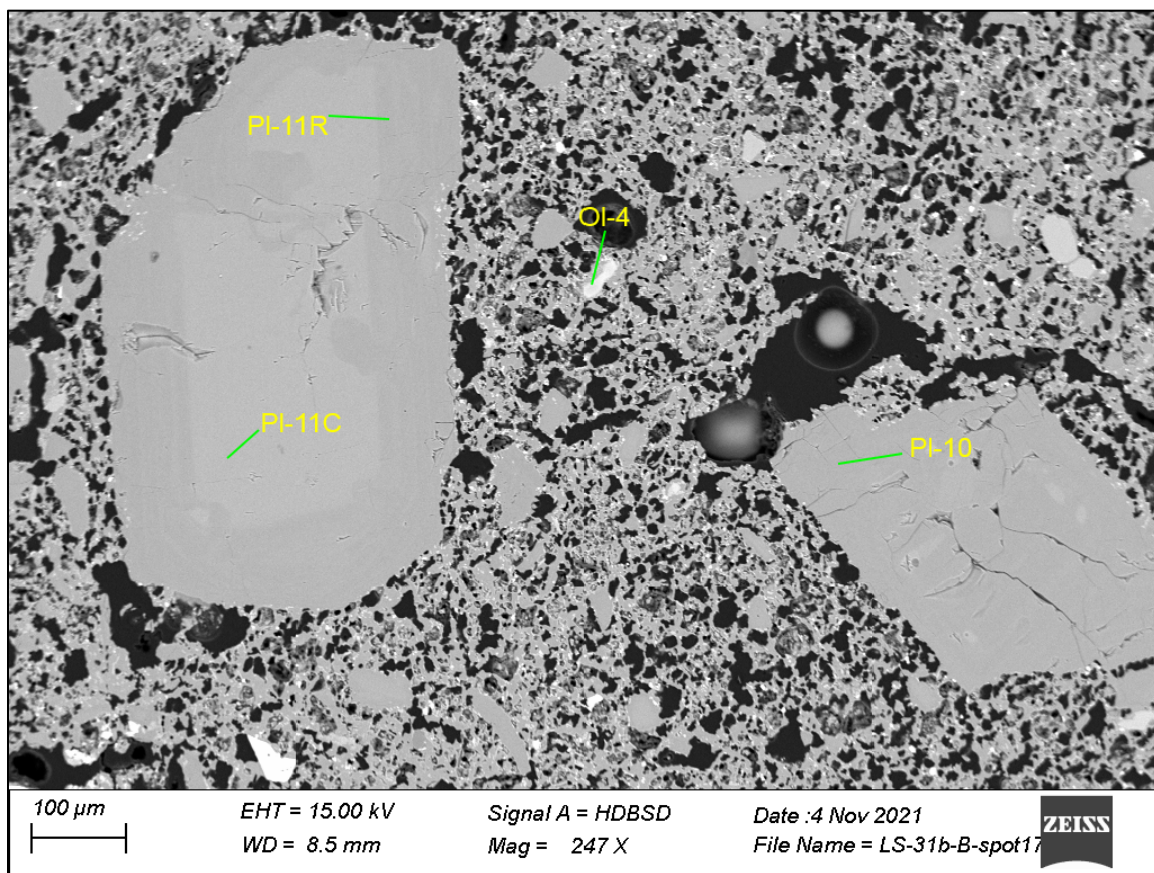


Figure 9. A BSE image from 21 showing plagioclase phenocrysts from U2 as euhedral and isolated, as well as both un-zoned (PL-10) and normally zone (PL-11).

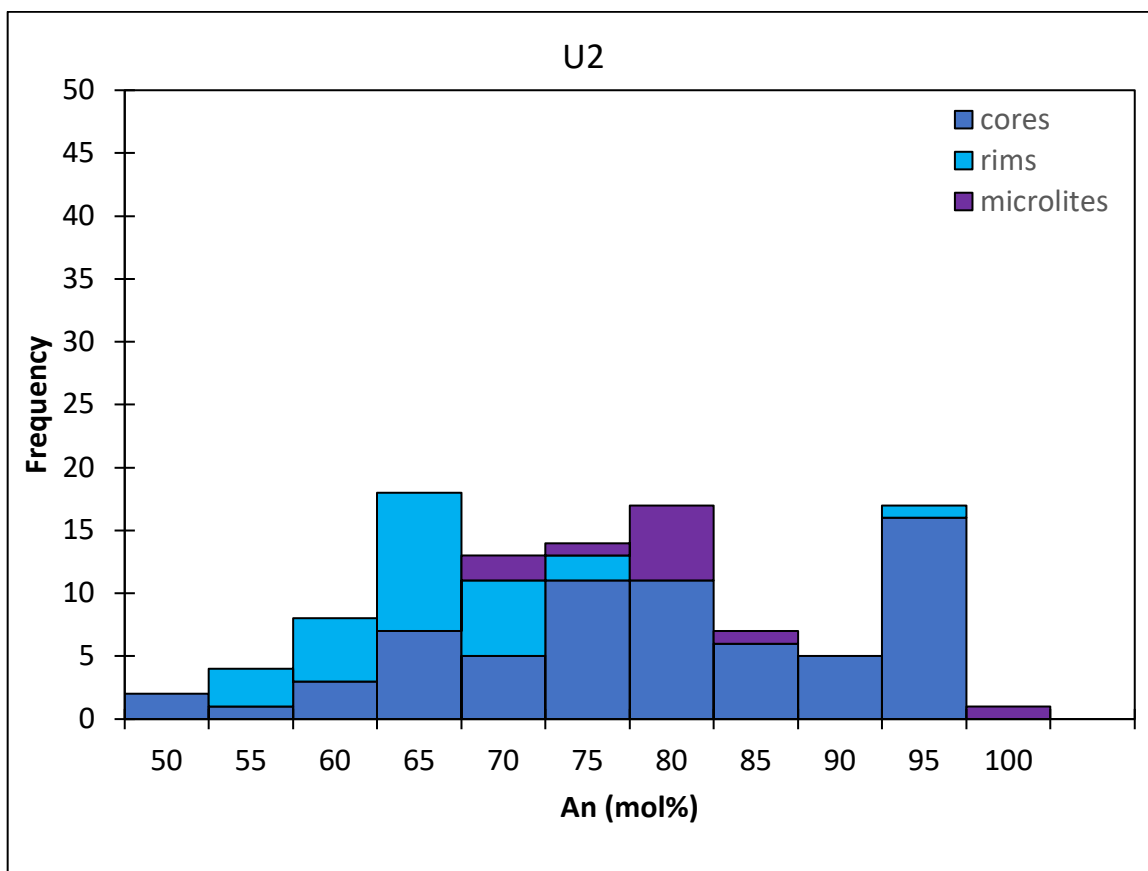


Figure 10. A histogram of plagioclase in U2 showing that phenocryst cores are largely calcic (An75-95) while rims remain largely sodic (An55-65), and that microlites are not as calcic as in U1.

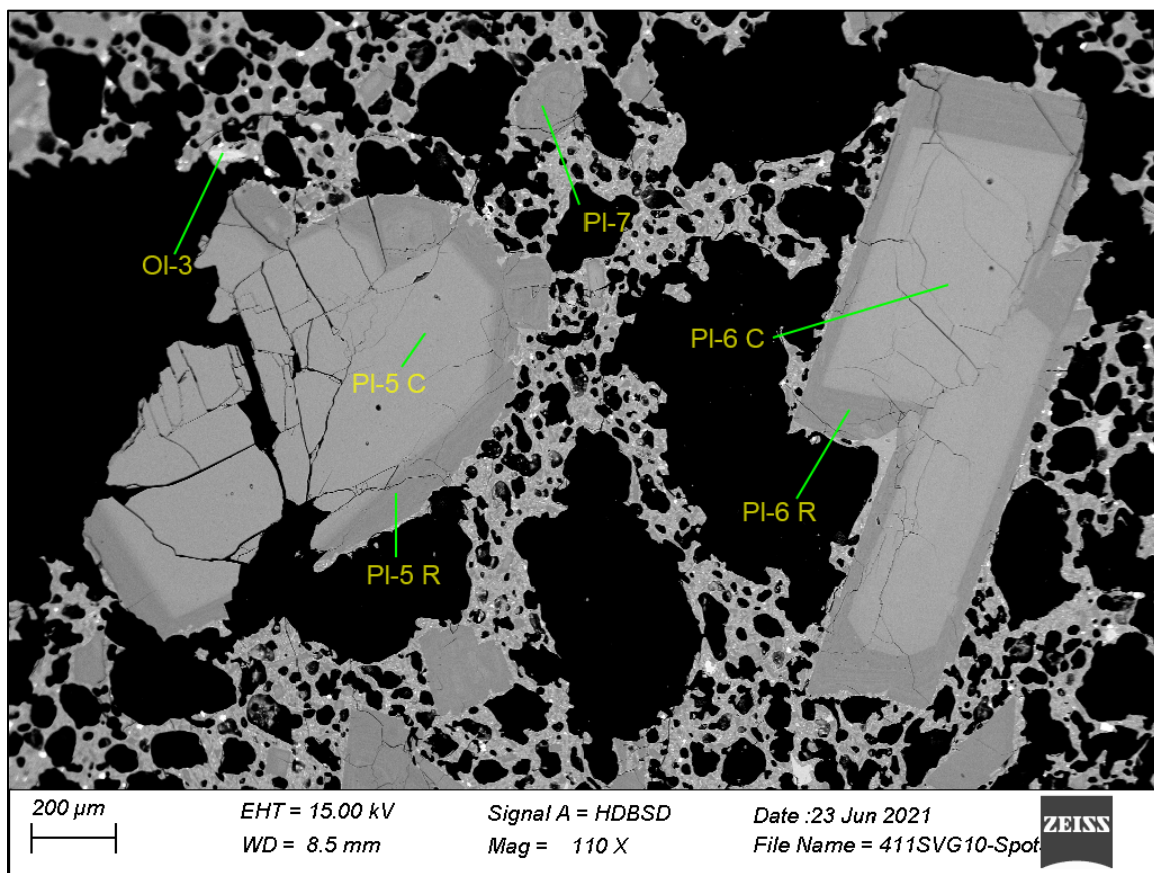


Figure 11. A BSE image of normally zoned plagioclase phenocrysts in U3, showing distinct calcic cores and thick sodic rims.

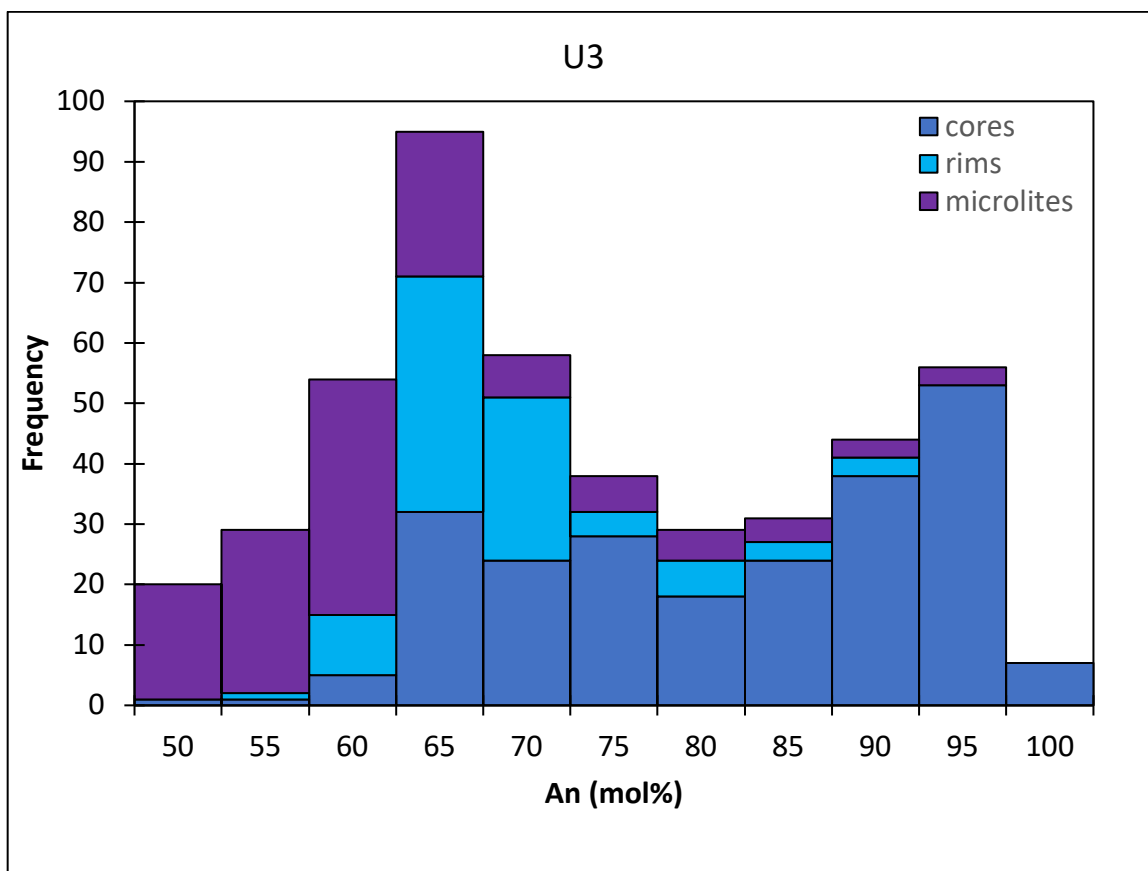


Figure 12. A plagioclase histogram from U3 showing the overall range of compositions, as well as phenocryst cores and rims that are comparable to U1 and U2. Distinctively, microlite compositions in U3 are more sodic (An_{45-65}) than the phenocryst rims (An_{60-70}).

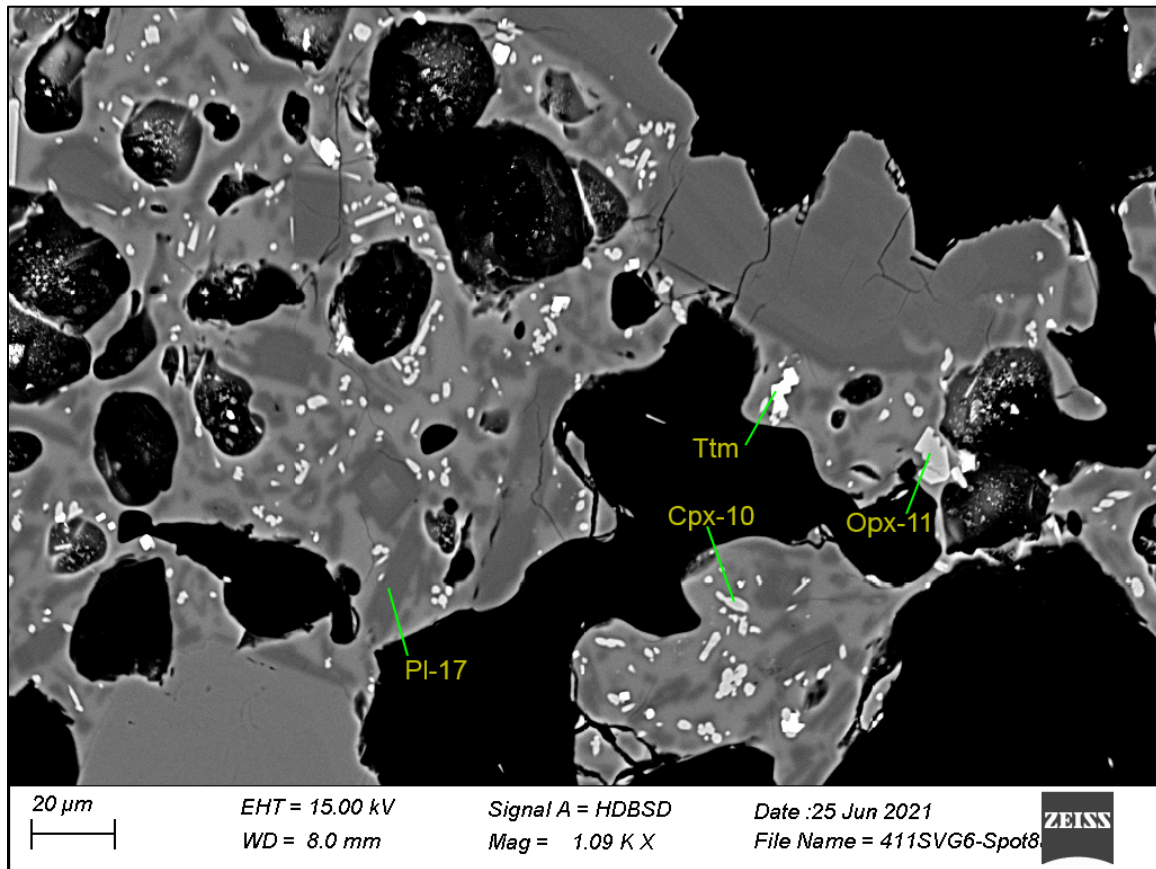


Figure 13. A BSE image of plagioclase microlites, as well as other mineral phases, growing in the melt.

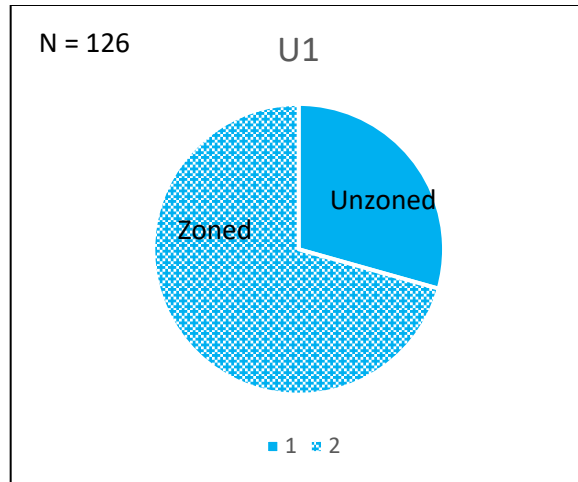


Figure 14. A pie chart showing the proportion of normally zoned plagioclase microlites and un-zoned plagioclase microlites in U1.

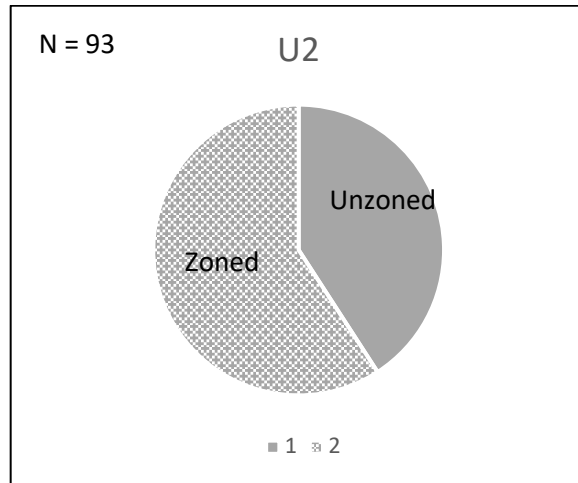


Figure 15. A pie chart showing the proportion of normally zoned plagioclase microlites and un-zoned plagioclase microlites in U2.

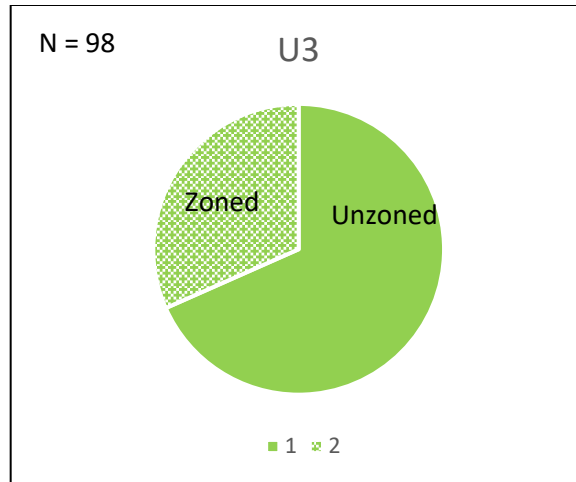


Figure 16. A pie chart showing the proportion of normally zoned plagioclase microlites and un-zoned plagioclase microlites in U3.

Plagioclase- FeO content and glomerocrysts

Plagioclase crystals contain minimal amounts of iron in their compositions, however it appears that over the course of the three eruptive phases, U1, U2, and U3, the Fe content increases for glomerocrysts while staying the same for isolated phenocrysts. Additionally, normally zoned microlites have relatively constant FeO content over the course of the first three eruptive phases while un-zoned microlites have higher and more variable FeO content (Fig. 17). In U1, the iron oxide content is approximately the same for both isolated phenocrysts and phenocrysts present in glomerocrysts (Fig. 18). In U2, the iron oxide content is slightly higher in the glomerocrysts than it is in the isolated phenocrysts (Fig. 19). In U3, the FeO content is even higher in the glomerocrysts, showing a clear difference between the isolated phenocrysts and glomerocrysts (Fig. 20). Additionally, normally zoned microlites show little variation in iron content (~0.6-0.9 wt%) in all samples, but a wide compositional range for anorthite content (~50-95 mol%). The un-zoned and Na-rich microlites show increased variability of iron content (~0.6-

1.4 wt%) in all three initial explosive phases, but a more limited anorthite compositional range (~45-60 mol%) (Fig. 17).

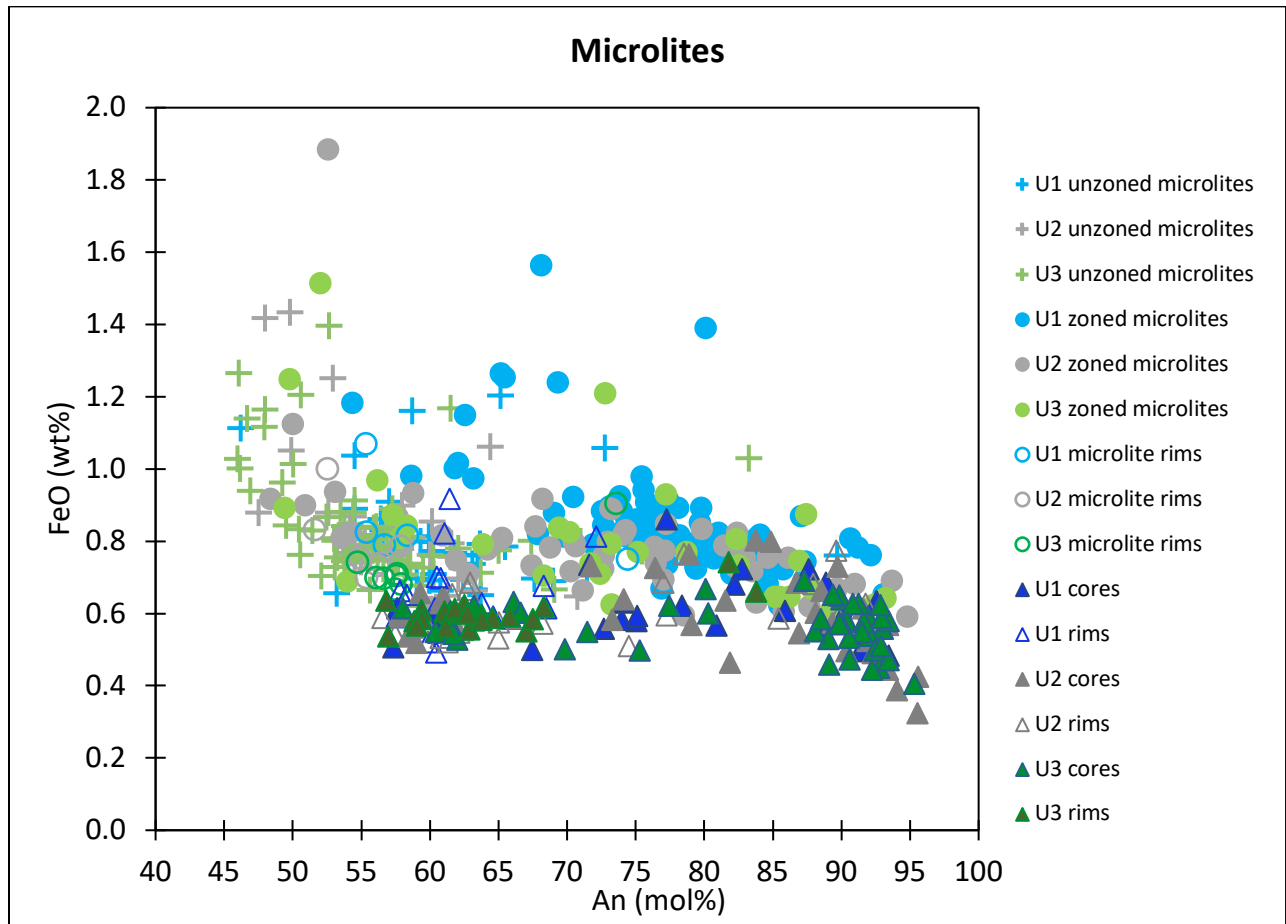


Figure 17. A scatter plot comparing the iron oxide content to the anorthite content of U1, U2, and U3 normally zoned phenocrysts, normally zoned microlites, and un-zoned microlites.

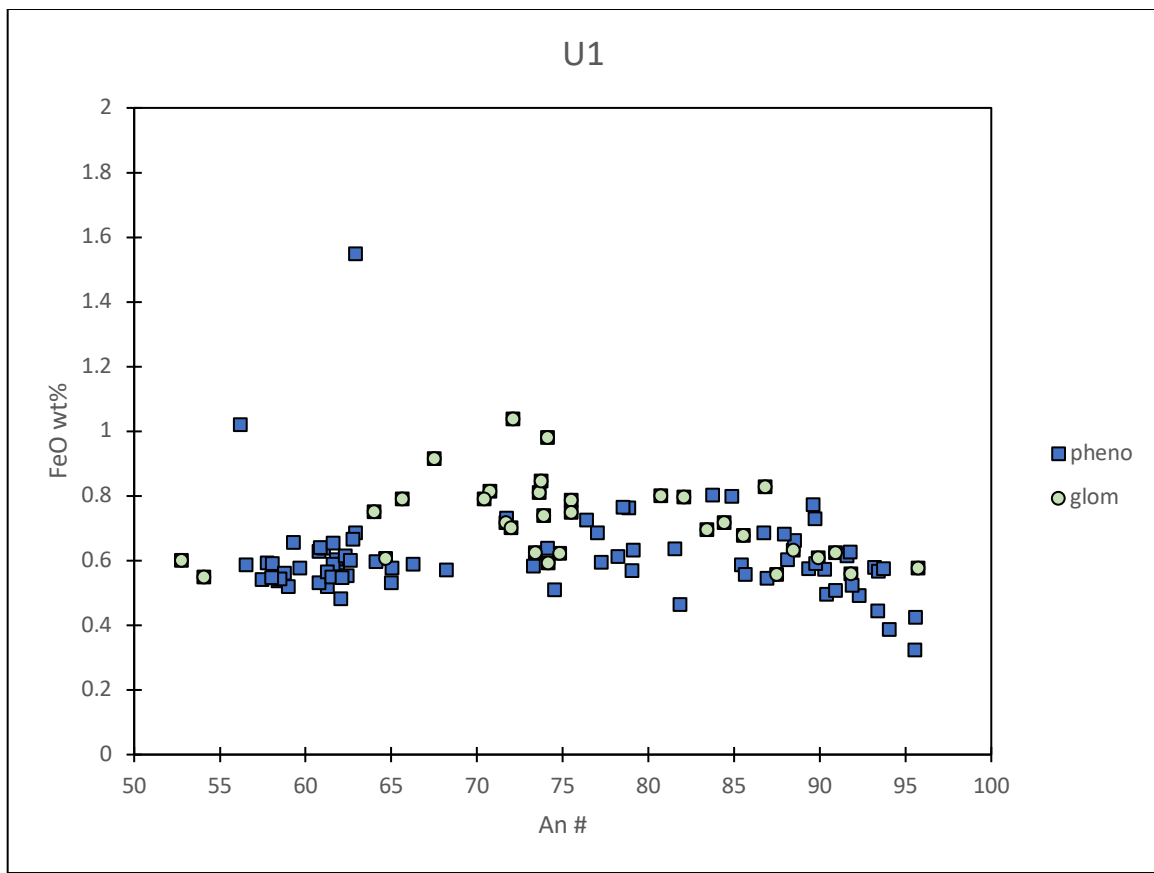


Figure 18. A scatter plot comparing the U2 iron oxide content in isolated plagioclase phenocrysts and plagioclase phenocrysts present in glomerocrysts.

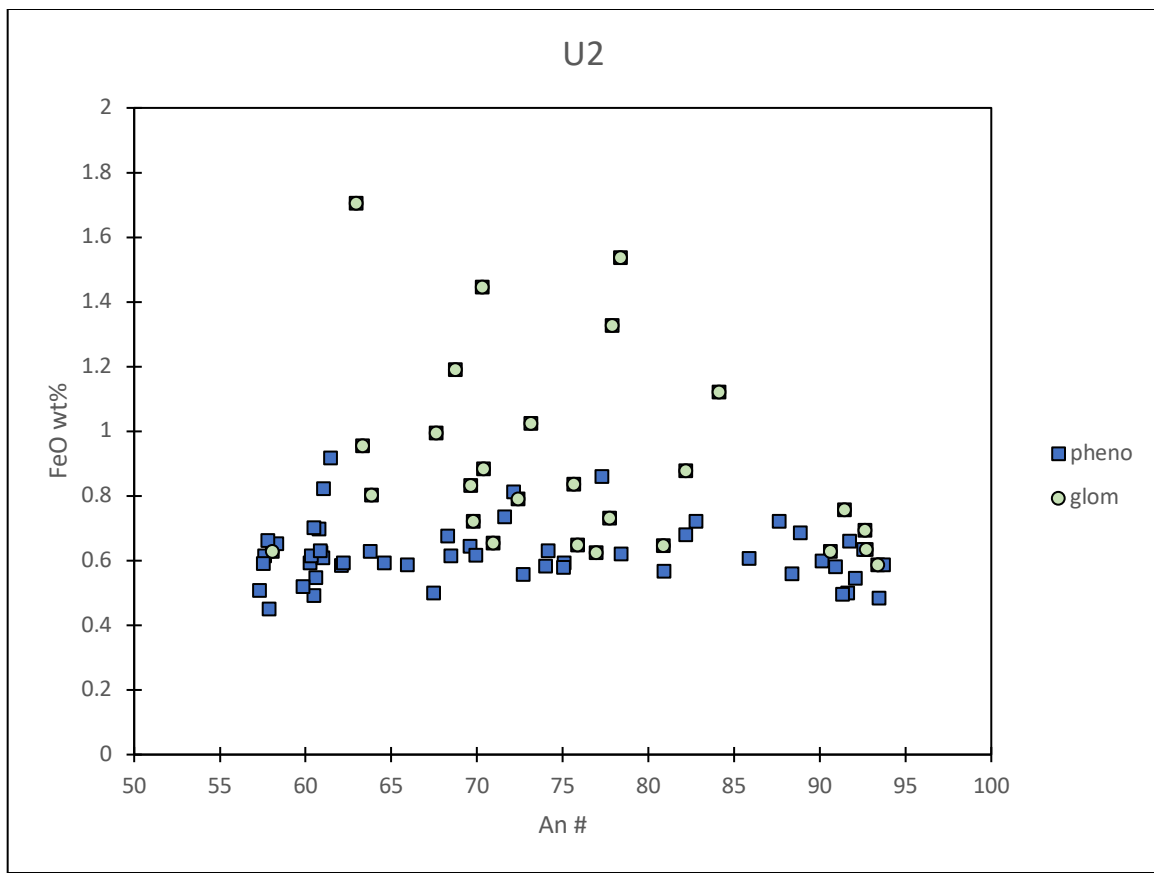


Figure 19. A scatter plot comparing the U2 iron oxide content in isolated plagioclase phenocrysts and plagioclase phenocrysts present in glomerocrysts.

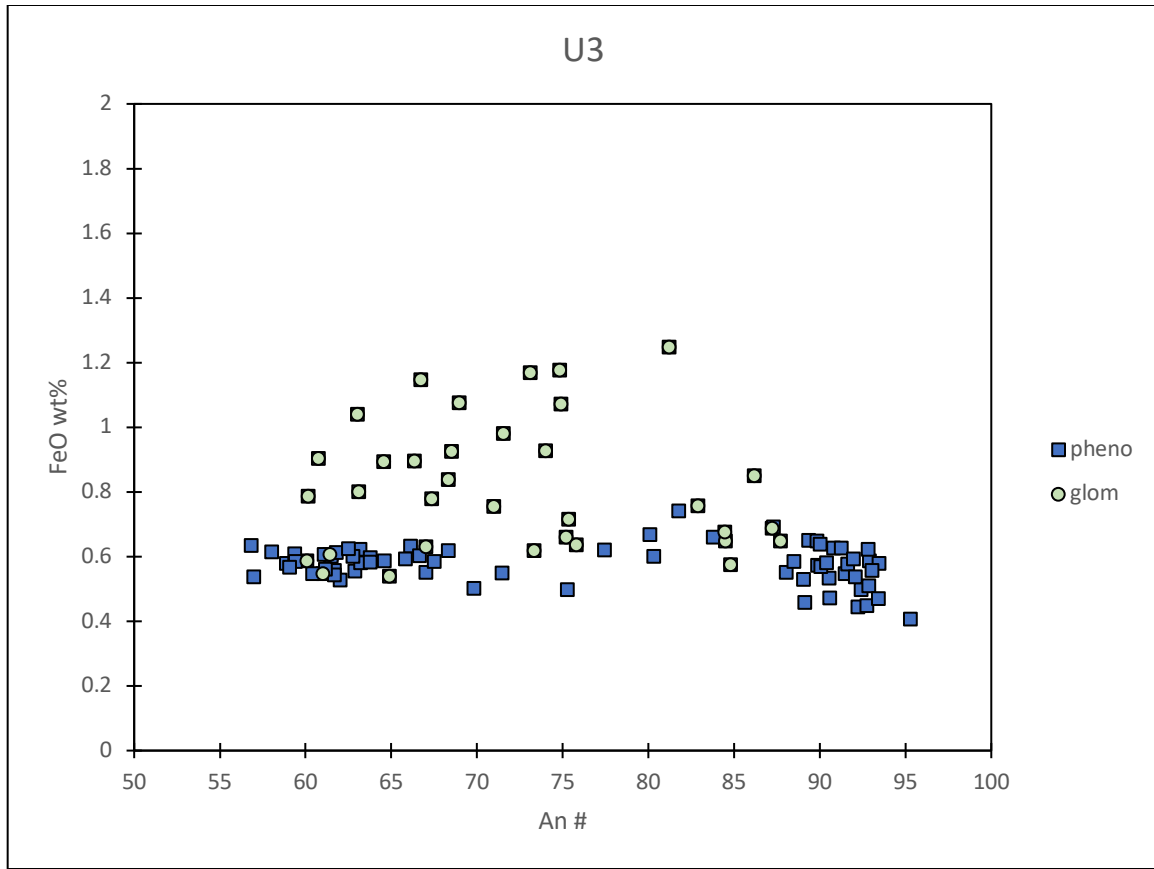


Figure 20. A scatter plot comparing the U3 iron oxide content in isolated plagioclase phenocrysts and plagioclase phenocrysts present in glomerocrysts.

Olivine- phenocrysts

Olivine occurs in U1, U2, and U3 and their abundance varies across the samples, being most abundant in U1 and least in U3. Olivine phenocrysts (100 μ m-1mm) in U1 are euhedral and largely un-zoned with compositions of Fo₆₅₋₈₀, however some have very thin (<5 μ m) Fe-rich rims that are too thin to analyze by SEM. Olivine is present as both isolated phenocrysts and with other phases as glomerocrysts (Fig. 21 and 22). Phenocrysts in U2 are euhedral and largely un-zoned with variable compositions (Fo₆₀₋₈₀), while also presenting as isolated and in glomerocrysts (Fig. 23 and 24). Fe-rich rims are also present in U2 but similar to U1, are too thin to get accurate analyses by SEM. Olivine phenocrysts in U3 occur as both euhedral and isolated,

as well as in glomerocrysts. Phenocrysts are largely un-zoned (Fo_{59-90}), however few have very thin Fe-rich rims are too thin to analyze by SEM and are likely inaccurate (Fig. 25 and 26).

Olivine- microlites

Olivine microlites occur in all samples from U1, U2, and U3, however they vary in abundance throughout the separate eruptive phases being most abundant in U1 and least in U3. There appears to be a relationship between the change in abundance of olivine microlites with the change in abundance of orthopyroxene microlites. Olivine microlites are abundant in U1 relative to orthopyroxene microlites and olivine compositions range from Fo_{60-80} (Fig. 22). In U2, olivine and opx microlite abundance are approximately equal and olivine compositions range from Fo_{60-80} , similar to U1 (Fig. 24). Olivine microlites are rare compared to opx microlites in U3 and cover a broader variety of compositions, ranging from Fo_{55-80} , similar to the compositions of the phenocrysts (Fig. 26).

Olivine- glomerocrysts

Olivine is present in glomerocrysts in all three eruptive phases, however, are most commonly found in glomerocrysts in U3 samples. Olivine in U1 glomerocrysts show a broad compositional range of Fo_{55-85} (Fig. 22). Olivine in U2 glomerocrysts show less variance in compositions (Fo_{65-75}) (Fig. 24). Olivine in U3 glomerocrysts show broad variety of compositions (Fo_{55-95}) with a large peak at Fo_{65-75} (Fig. 26).

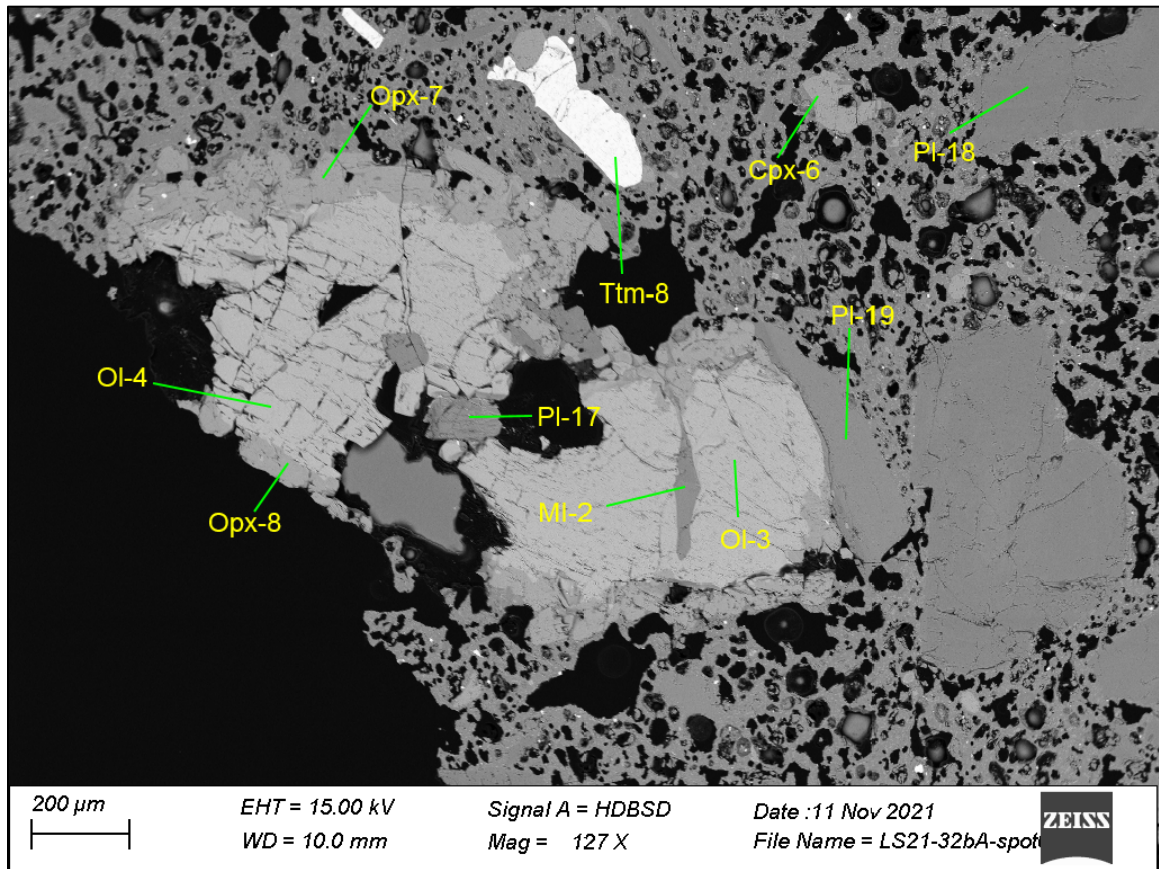


Figure 21. A BSE image of an un-zoned olivine phenocryst in U1, occurring with other mineral phases as a cumulate xenolith.

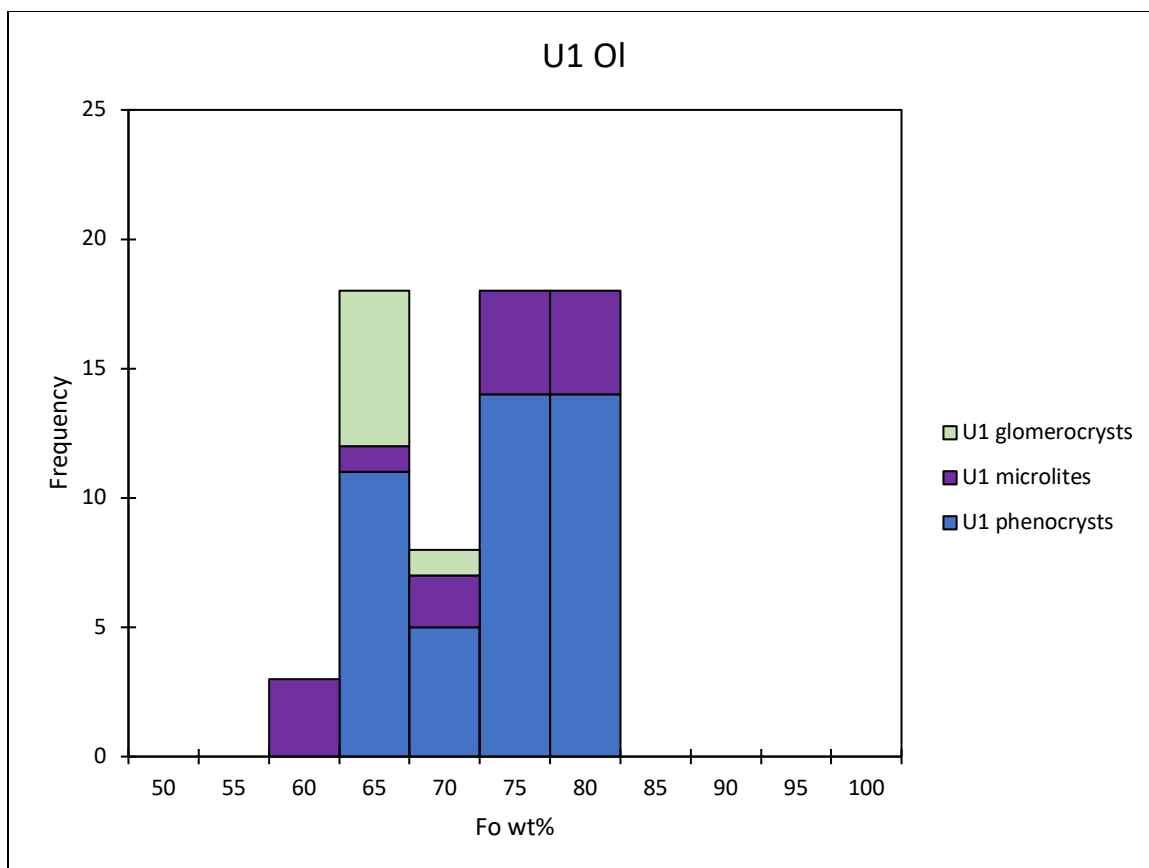


Figure 22. A histogram of olivine in U1, showing the compositional ranges of both un-zoned phenocrysts, phenocrysts present in glomerocrysts, and microlites.

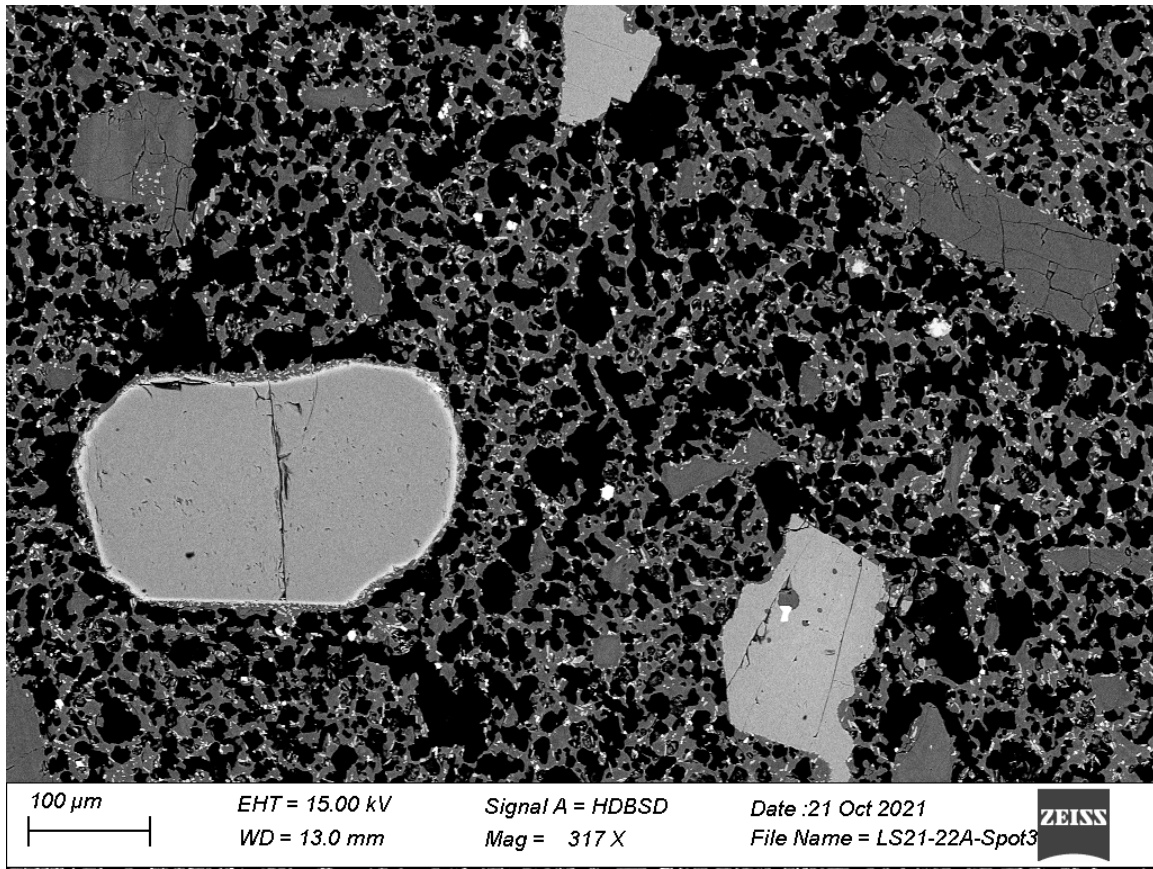


Figure 23. A BSE image from U2 of a zoned olivine occurring among other isolated mineral phases in the melt.

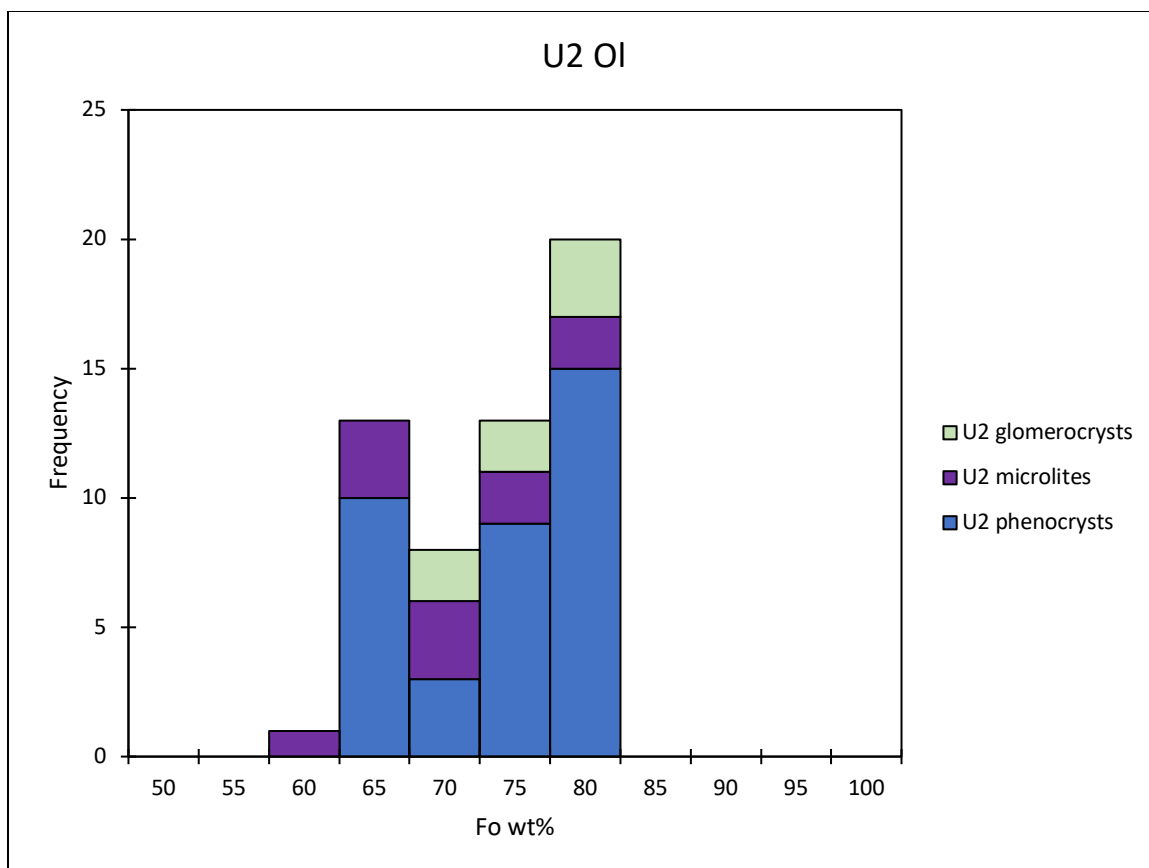


Figure 24. A histogram of olivine phenocrysts (isolated and in glomerocrysts) and microlites in U2, showing compositional ranges of each.

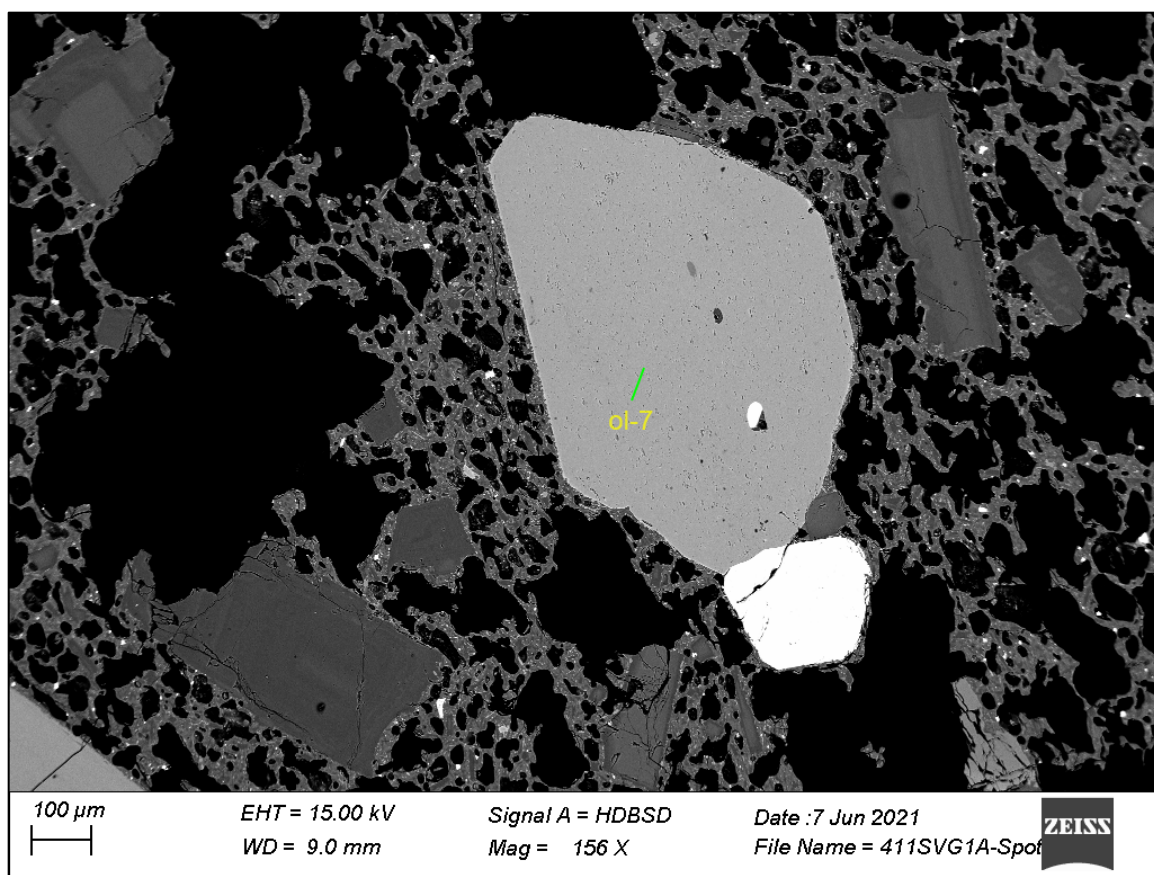


Figure 25. A BSE from U3 of a euhedral and isolated phenocryst.

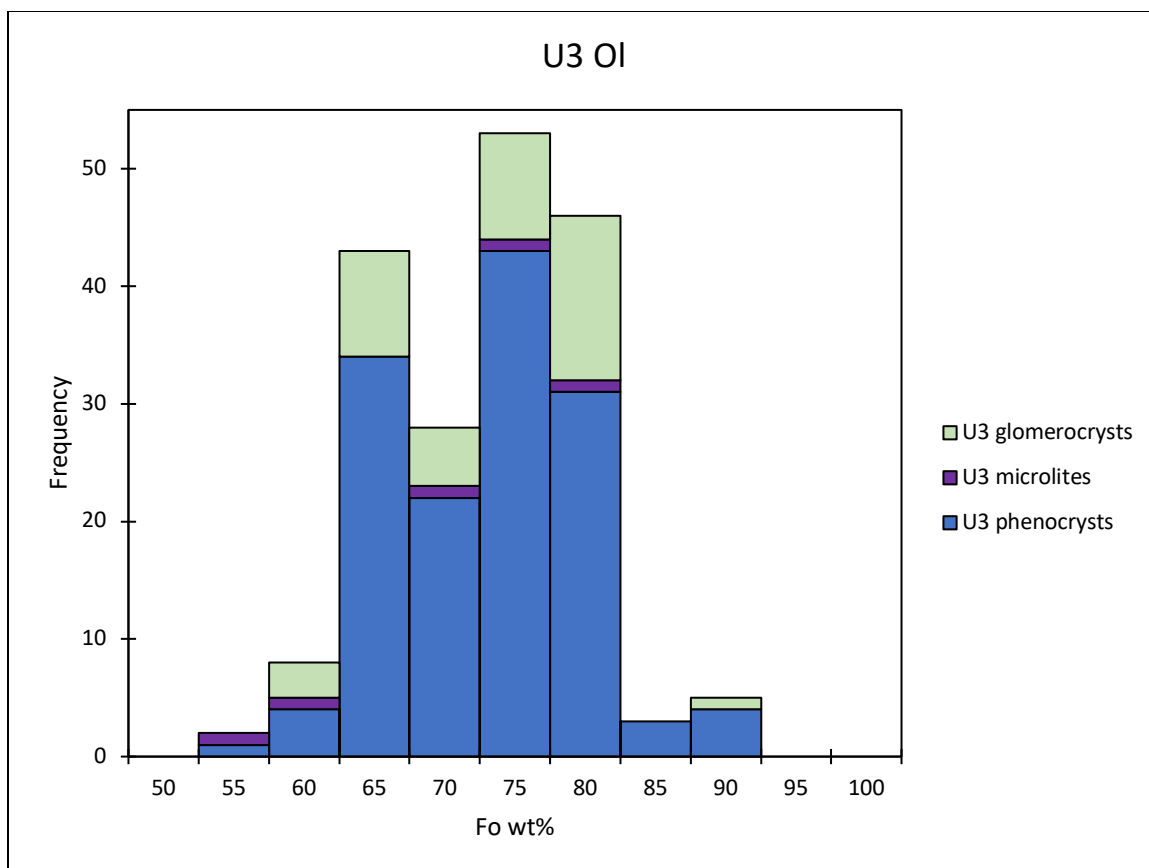


Figure 26. A histogram depicting the compositional range and frequency of olivine in U3. Phenocrysts are largely un-zoned but appear both isolated and in glomerocrysts. Microlite compositions do not vary outside of phenocryst compositions.

Clinopyroxene (Cpx)- phenocrysts

Clinopyroxene crystals are present in all eruptive phases as euhedral and un-zoned phenocrysts (100 μ m-1mm). Cpx phenocrysts in U1 occur as isolated and as part of glomerocrysts and they are largely un-zoned (Fig. 27). Phenocryst compositions range from Mg# 0.65-0.80 with very few rims that range Mg# 0.70-0.80 (Fig. 28). Cpx phenocrysts in U2 occur as isolated and euhedral, as well as included in other mineral phases, yet they remain compositionally similar to cpx phenocrysts observed in U1 samples, ranging from Mg# 0.70-0.75 (Fig. 29 and 30). There is minimal zoning of cpx in U2, but the very few rim compositions are Mg# 0.75-0.8 (Fig. 30). Cpx phenocrysts that are in U3 samples are euhedral and occur as isolated crystals, as part of glomerocrysts, and are both zoned and un-zoned (Fig. 31). Un-zoned

phenocrysts, and the cores of those that are normally zoned, have compositions that range Mg# 0.65-0.90 while the very few normally zoned rims have compositions that range Mg# 0.75-0.85 (Fig. 32).

Clinopyroxene (Cpx)- microlites

Clinopyroxene microlites occur in all samples from U1, U2, and U3 and are relatively equal in abundance throughout all eruption phases. Microlite compositions in U1 vary slightly with a range of Mg# 0.65-0.8 whereas the compositions in U2 and U3 show greater variance. Microlite compositions in U2 show a more Fe-rich and broader range of Mg# 0.5-0.8 while U3 compositions show a broad range of Mg# 0.55-0.75 that correlates similarly with phenocryst compositions. Microlites appear more Fe-rich than phenocrysts in U2 and U3 than in U1 (Fig. 28, 30, 32).

Clinopyroxene (Cpx)- glomerocrysts

Clinopyroxene is present in glomerocrysts in all three eruptive phases but are most commonly found in glomerocrysts in U3 samples. Cpx in U1 glomerocrysts show the same compositional range as isolated phenocrysts (Mg# 0.65-0.80) (Fig. 28). Phenocrysts in U2 glomerocrysts also show the same compositional range as isolated phenocrysts (Mg# 0.70-0.75), and those present in U3 glomerocrysts continue to show the same compositional range as isolated phenocrysts (Mg# 0.65-0.90) (Fig. 30 and 32).

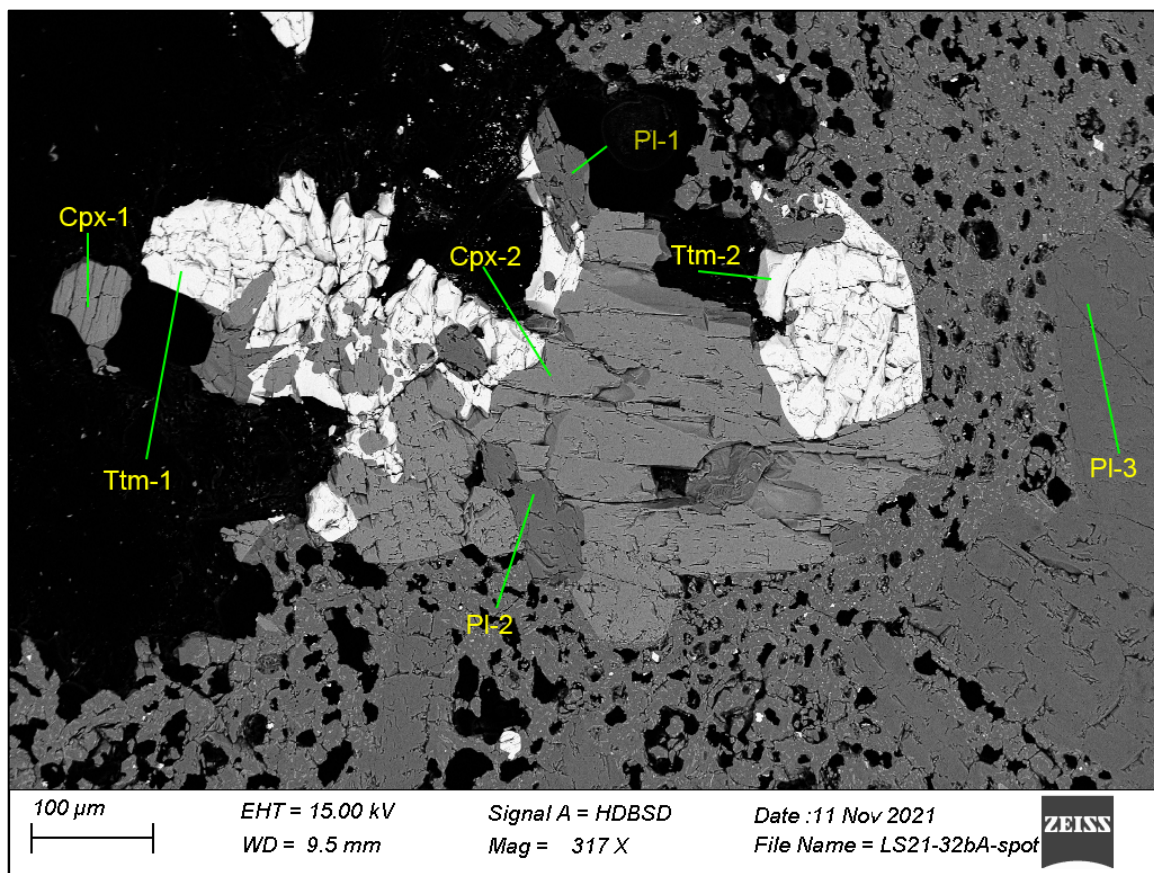


Figure 27. A BSE image of clinopyroxene in a U1 sample occurring as part of a shattered glomerocryst.

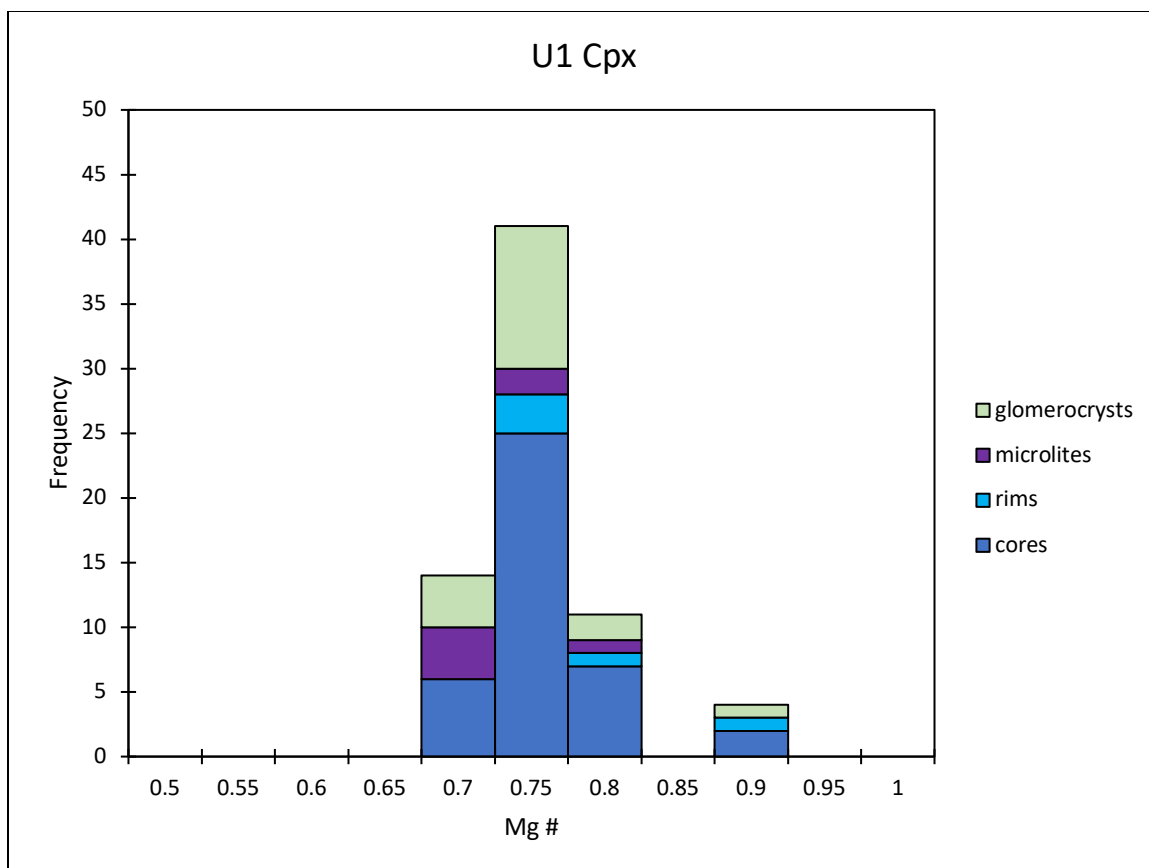


Figure 28. A histogram of clinopyroxene phenocrysts and microlites from U1 showing that zoned and un-zoned phenocryst and microlite compositions range from Mg# 0.65-0.80.

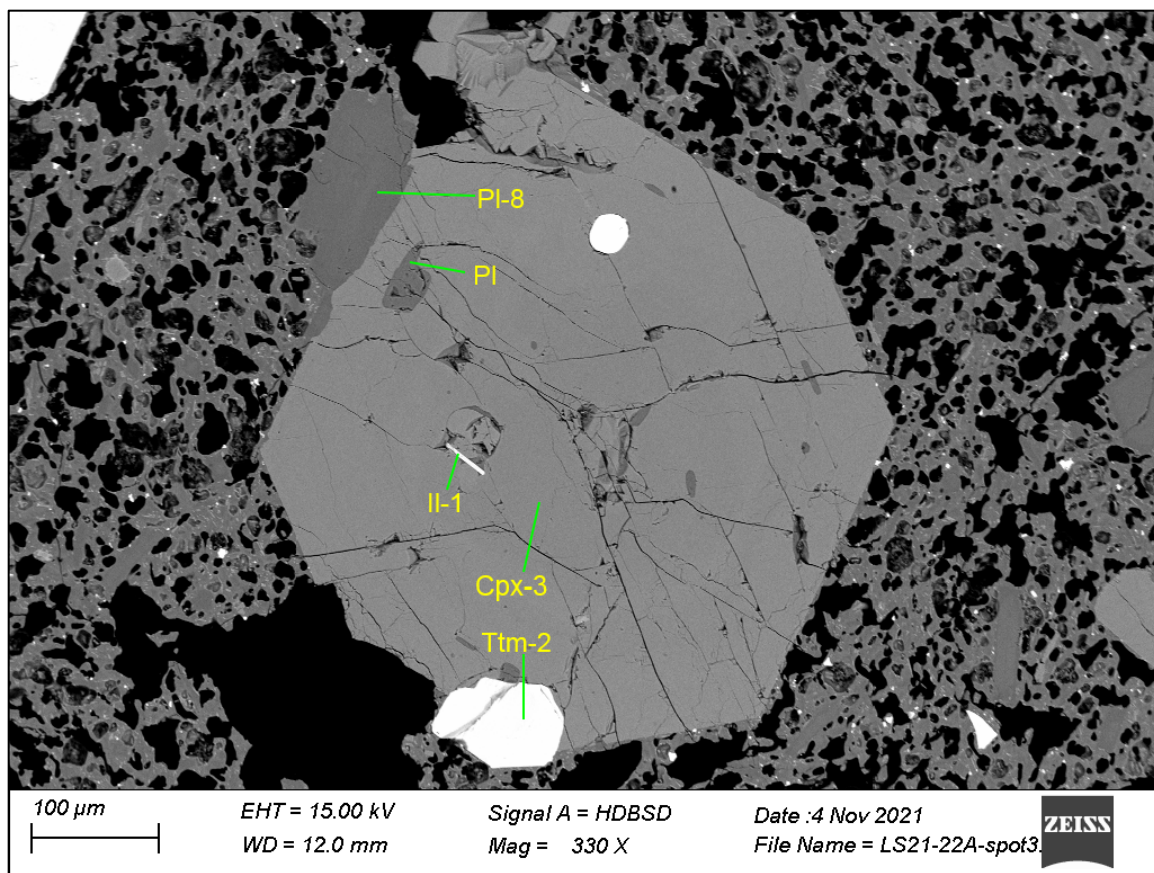


Figure 29. A BSE image of a euhedral and isolated clinopyroxene phenocryst in a U2 sample.

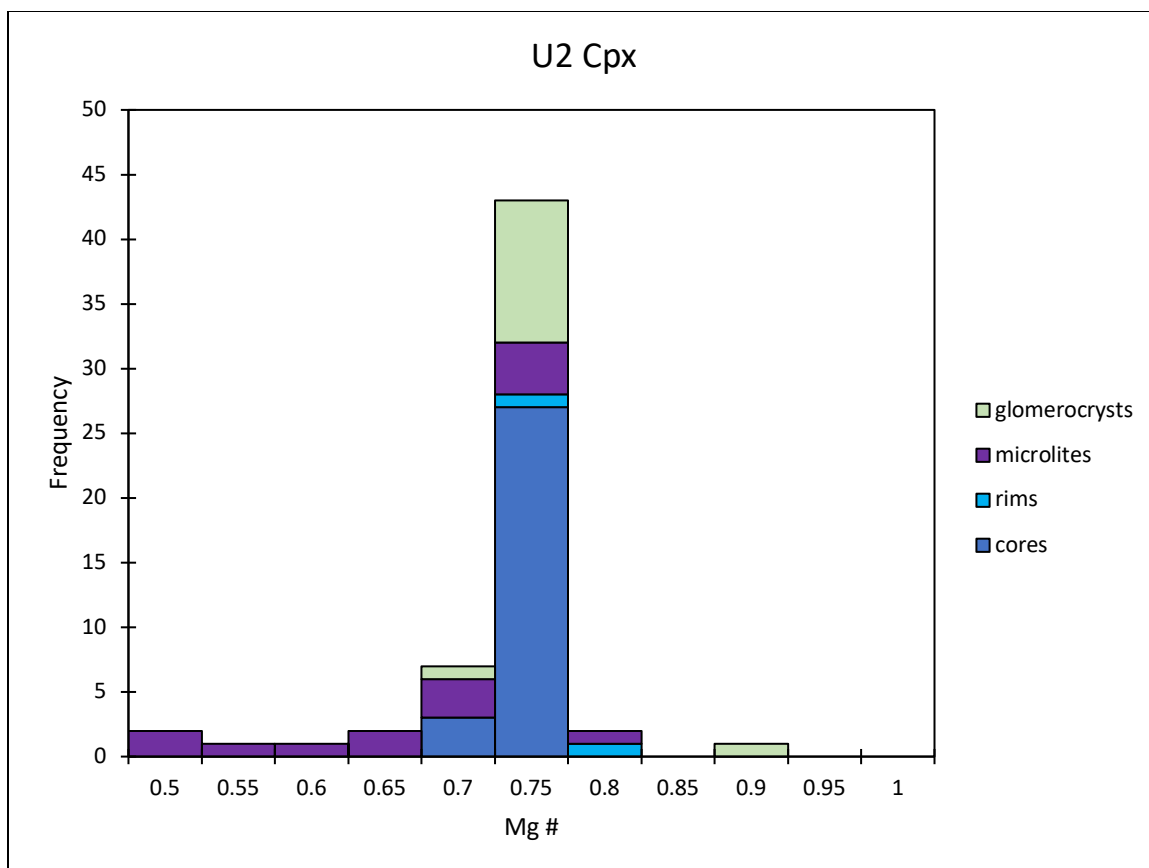


Figure 30. A histogram of clinopyroxene phenocryst and microlite compositions from U2 in which phenocrysts have a peak at Mg# 0.70-0.75, whereas microlites are more Fe-rich.

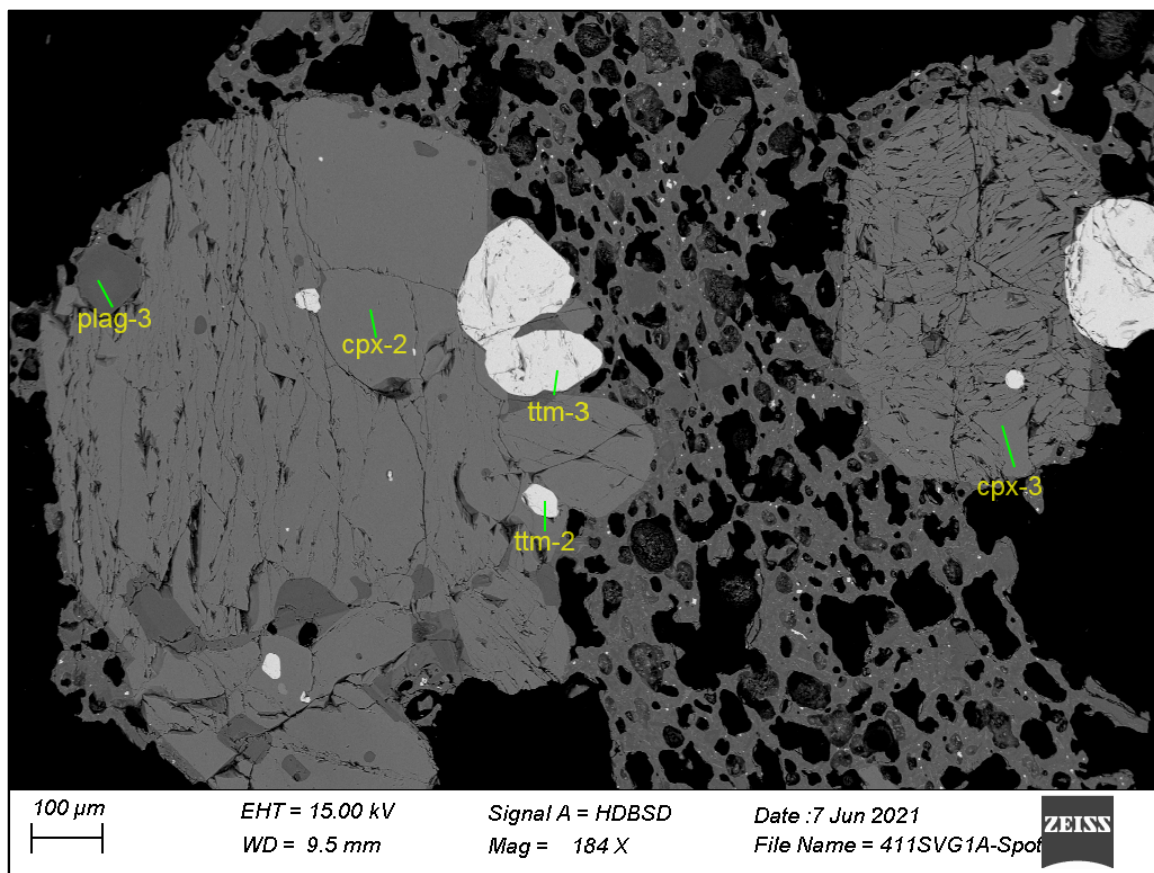


Figure 31. A BSE image of clinopyroxene phenocrysts in U3, occurring both in isolation and among other phases in a glomerocryst.

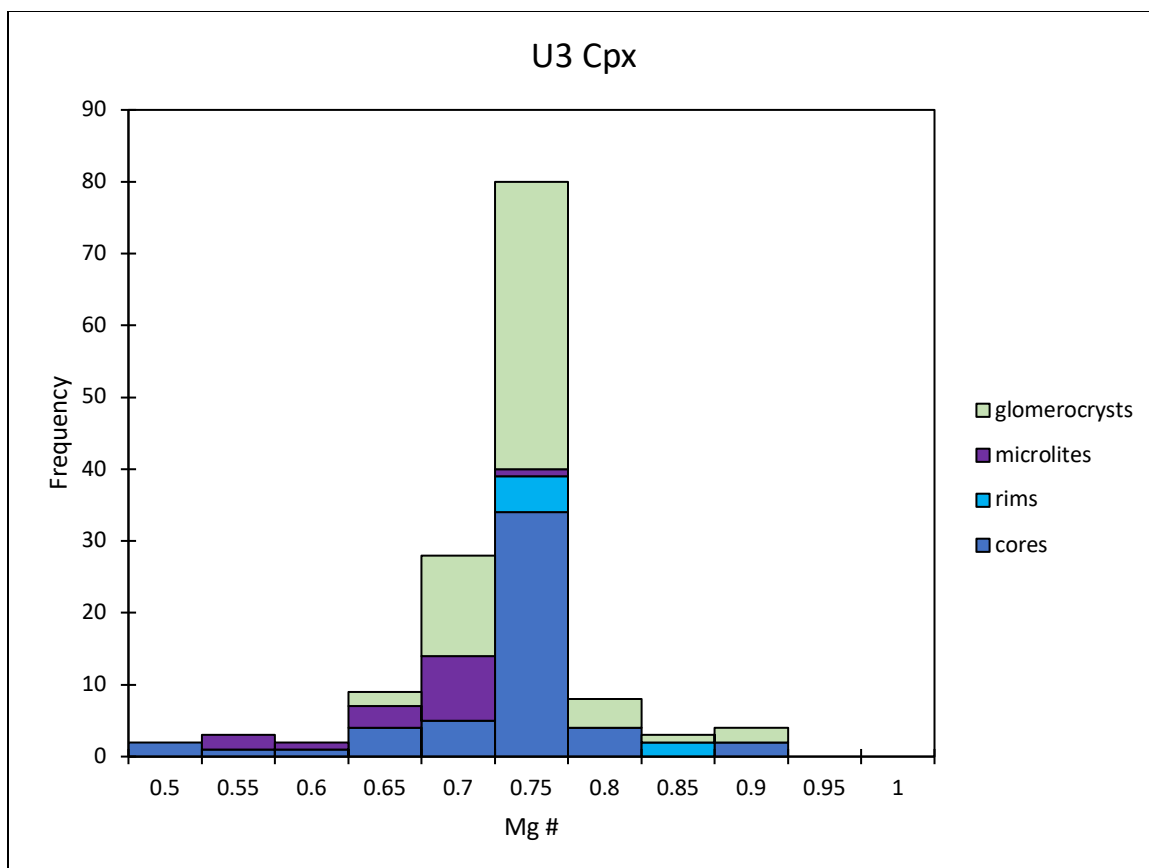


Figure 32. A histogram of clinopyroxene phenocrysts, microlites, and glomerocrysts in U3, showing that phenocryst and glomerocryst compositions peak at Mg# 0.70-0.75, but span a large range (Mg# 0.50-0.90), while microlites are more Fe-rich (Mg# 0.55-0.70).

Orthopyroxene (Opx)- phenocrysts

Orthopyroxene crystals are present in all samples from U1, U2, and U3 and are commonly seen as isolated phenocrysts or as part of glomerocrysts. Phenocrysts (100 μ m-1mm) are euhedral and show no evidence of disequilibrium textures (sieve textures or coronas) or zoning patterns (Fig. 33). Additionally, phenocrysts show little variation in compositions in all samples. Opx phenocrysts compositions in U1 show a range of Mg# 0.65-0.75 with a large peak at Mg# 0.70 (Fig. 34). Compositions of euhedral and un-zoned phenocrysts are similar in U2, however all compositions fall within the range of Mg# 0.65-0.70 (Fig. 35 and 36). Opx phenocrysts in U3 are minimally zoned, but mostly un-zoned and isolated with few as part of

glomerocrysts (Fig. 37). Phenocrysts show similar compositions to U1 and U2 with compositions ranging Mg# 0.5-0.80 with a peak at Mg# 0.70 (Fig. 38).

Orthopyroxene (Opx)- microlites

Orthopyroxene microlites are present in all samples from the three different eruptive phases (Fig. 39). Similar to the olivine microlites, opx microlites show the opposite trend in abundance in which they are least abundant in U1 and most abundant in U3. While opx microlites are less abundant than olivine in U1, they are equally as abundant cpx. The compositions of opx microlites in U1 appear to be Fe-rich with a range of Mg# 0.60-0.65 (Fig. 34). Microlites in U2 show more variable compositions than in U1 (Mg# 0.60-0.75), but opx and cpx microlites remain similar in abundance (Fig. 36). Microlites in U3 are more Fe-rich (Mg# 0.55-0.65) than phenocrysts and opx microlites are more abundant than cpx microlites (Fig. 38).

Orthopyroxene (Opx)- glomerocrysts

Orthopyroxene is present in glomerocrysts in all three eruptive phases, however, is most commonly found in glomerocrysts in U3 samples. Orthopyroxene in U1 glomerocrysts show the same compositional range as isolated phenocrysts (Mg# 0.65-0.80) (Fig. 33). Phenocrysts in U2 glomerocrysts also show the same compositional range as isolated phenocrysts (Mg# 0.70-0.75), and those present in U3 glomerocrysts continue to show the same compositional range as isolated phenocrysts (Mg# 0.65-0.90) (Fig. 36 and 38).

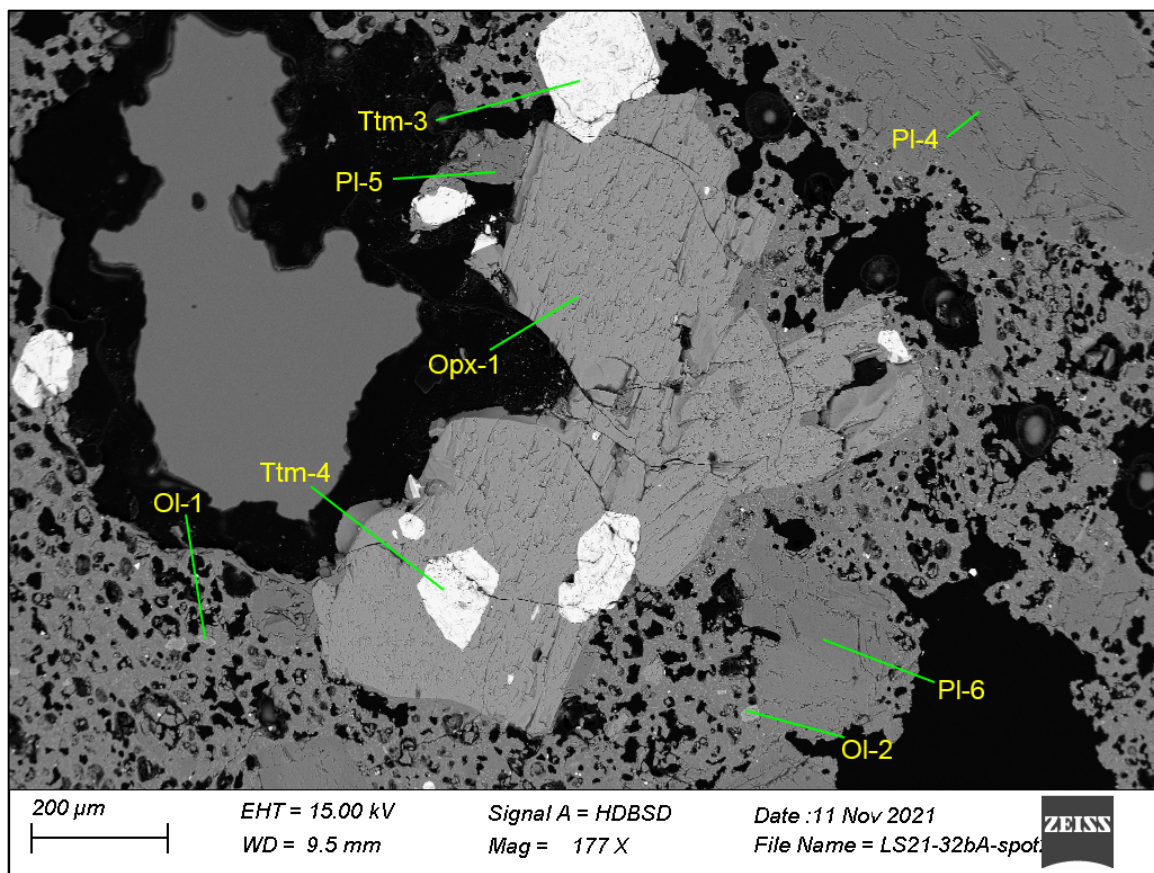


Figure 33. A BSE image of an orthopyroxene phenocryst in U1 that is euhedral and among other mineral phases.

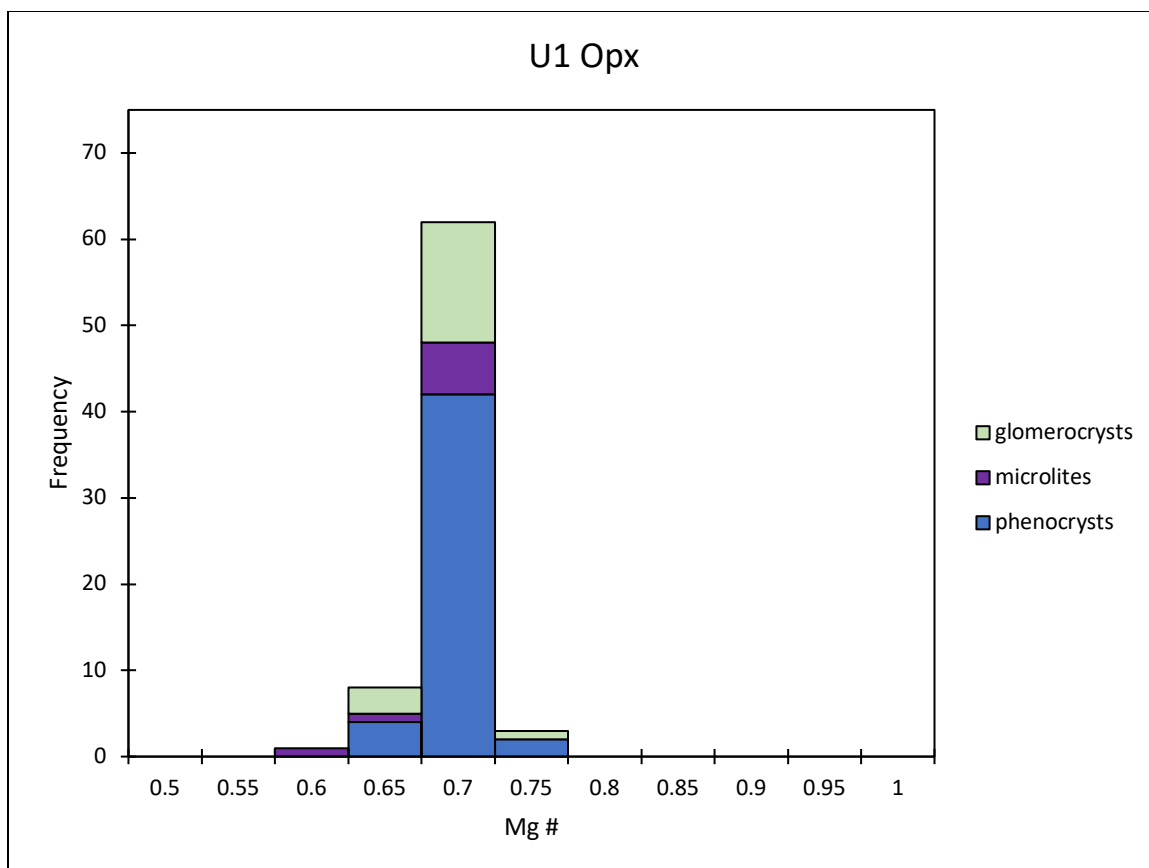


Figure 34. A histogram comparing orthopyroxene phenocryst and microlite compositions in U1, showing that phenocrysts are more Mg-rich (Mg# 0.65-0.75), whereas microlites are more Fe-rich, (Mg# 0.6-0.65).

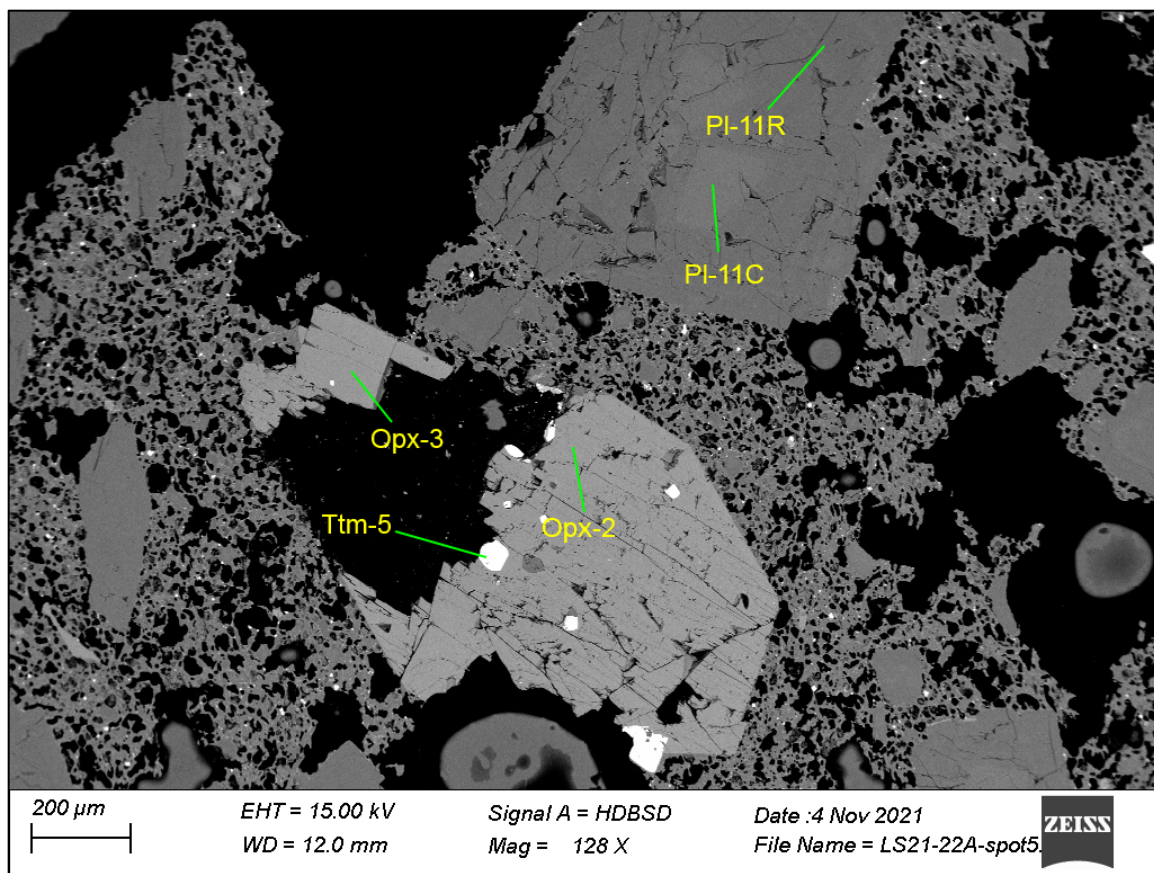


Figure 35. A BSE image of an isolated, euhedral, and un-zoned orthopyroxene phenocryst in U2 that has been shattered by the force of the eruption.

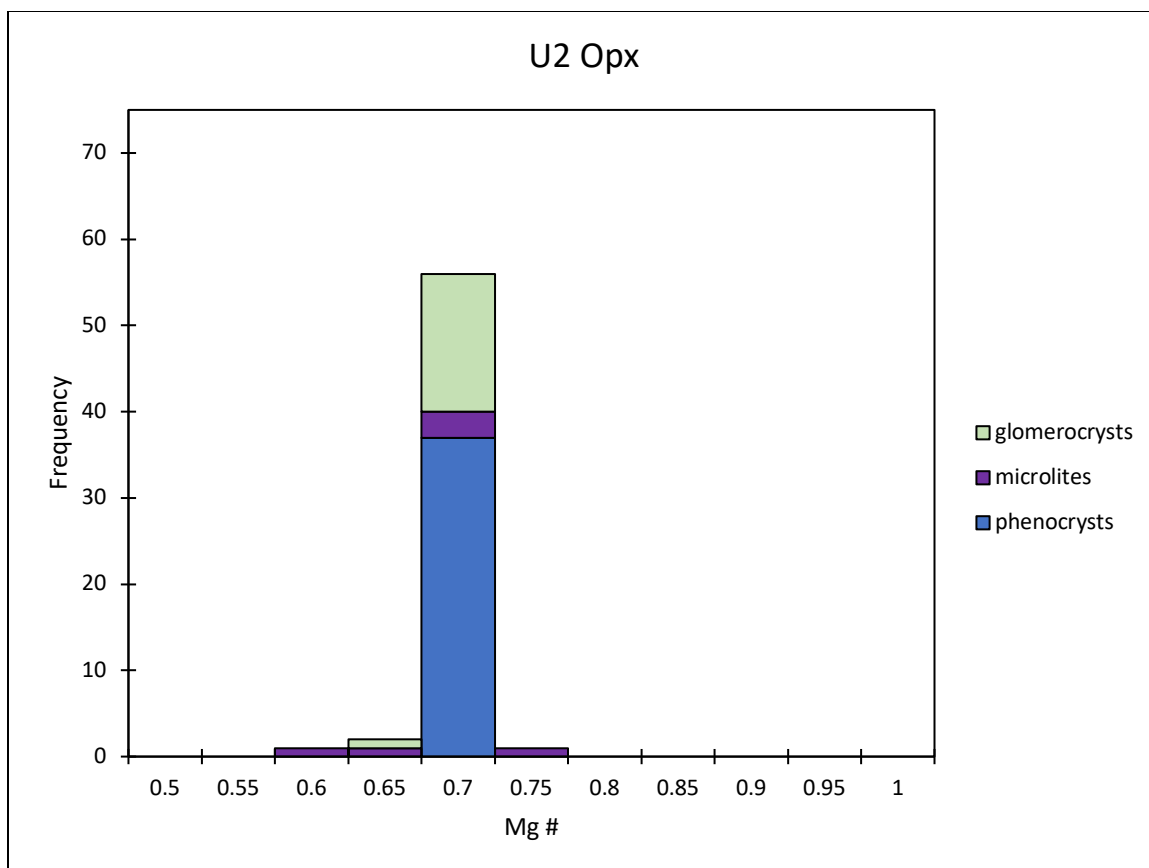


Figure 36. A histogram comparing orthopyroxene phenocryst, glomerocryst, and microlite compositions from U2, showing that phenocrysts and glomerocrysts have little variation (Mg# 0.65-0.7), whereas microlites are more variable (Mg# 0.60-0.75).

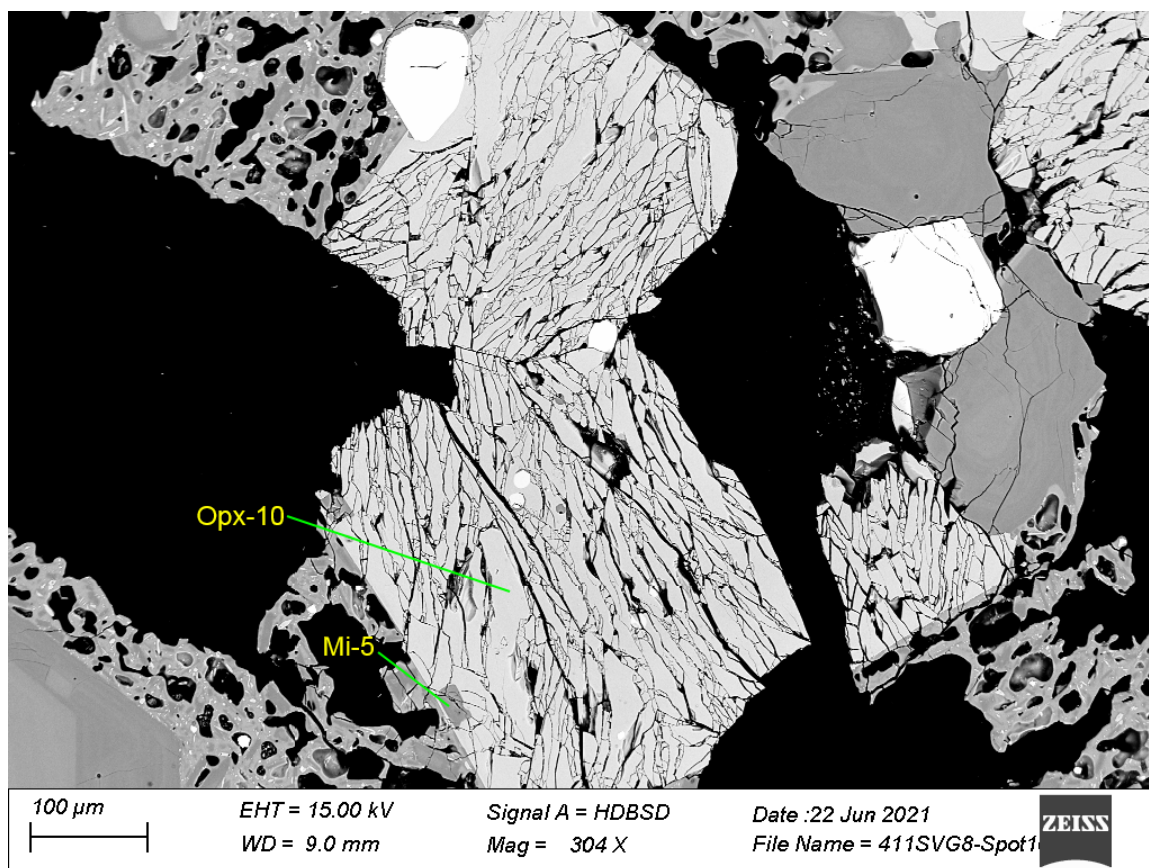


Figure 37. A BSE image of isolated and euhedral orthopyroxene phenocrysts in U3.

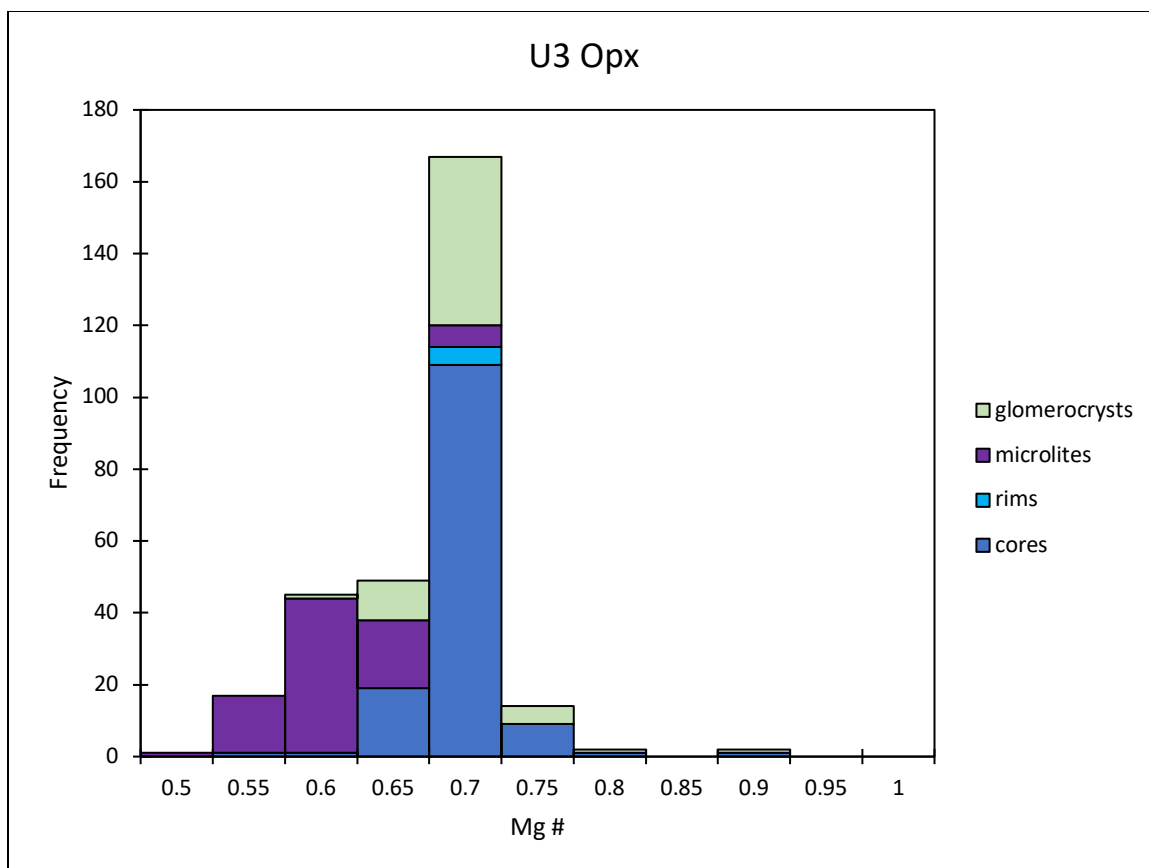


Figure 38. A histogram showing differences in compositions between orthopyroxene phenocrysts, glomerocrysts, and microlites in U3. Phenocrysts and cores are more Mg-rich whereas microlites are more Fe-rich.

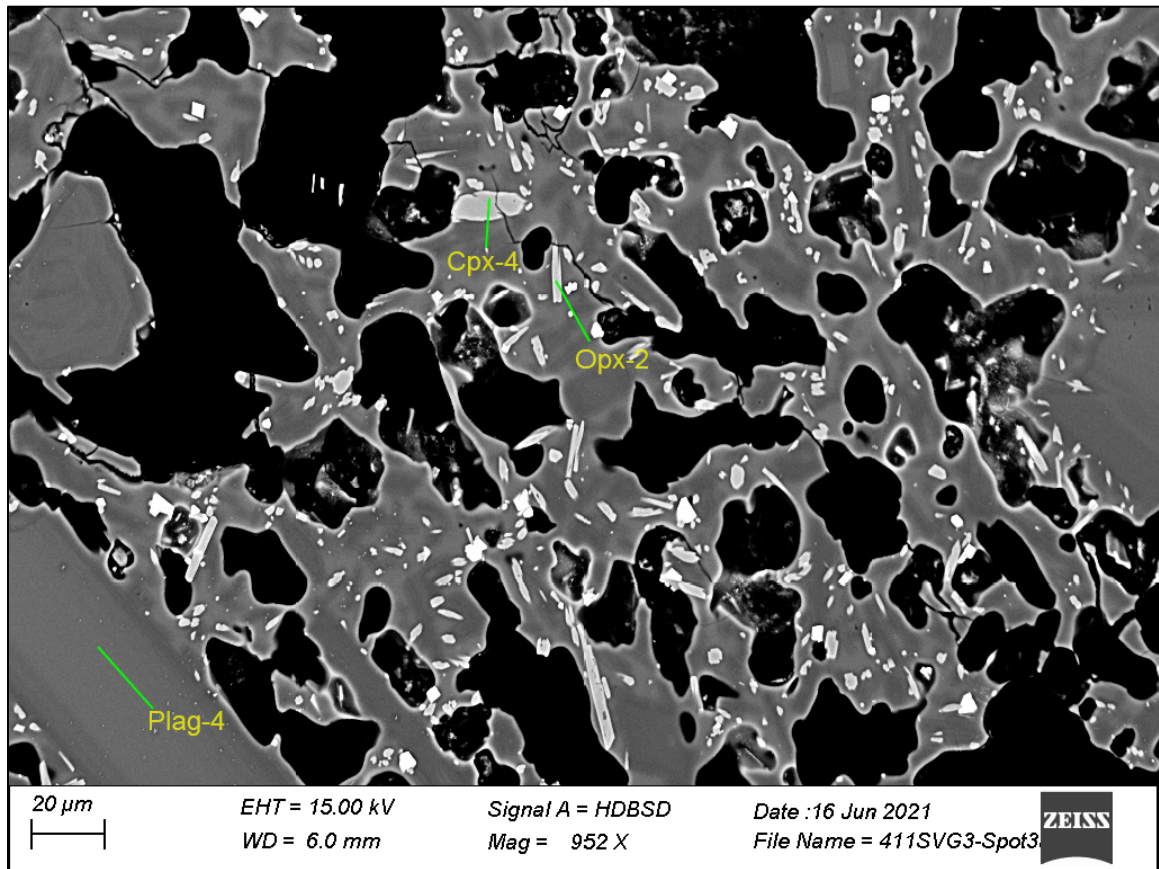


Figure 39. A BSE image of an orthopyroxene microlite in the melt from U3.

Titanomagnetite

Titanomagnetite crystals are present in all samples from U1, U2, and U3 and are uniform in composition throughout each eruptive phase. Phenocrysts are euhedral and un-zoned, occurring isolated and as part of glomerocrysts (Fig. 40, 41, and 42). Ttm phenocryst compositions in all three eruptive phases have a range of Mg# 0.02-0.10.

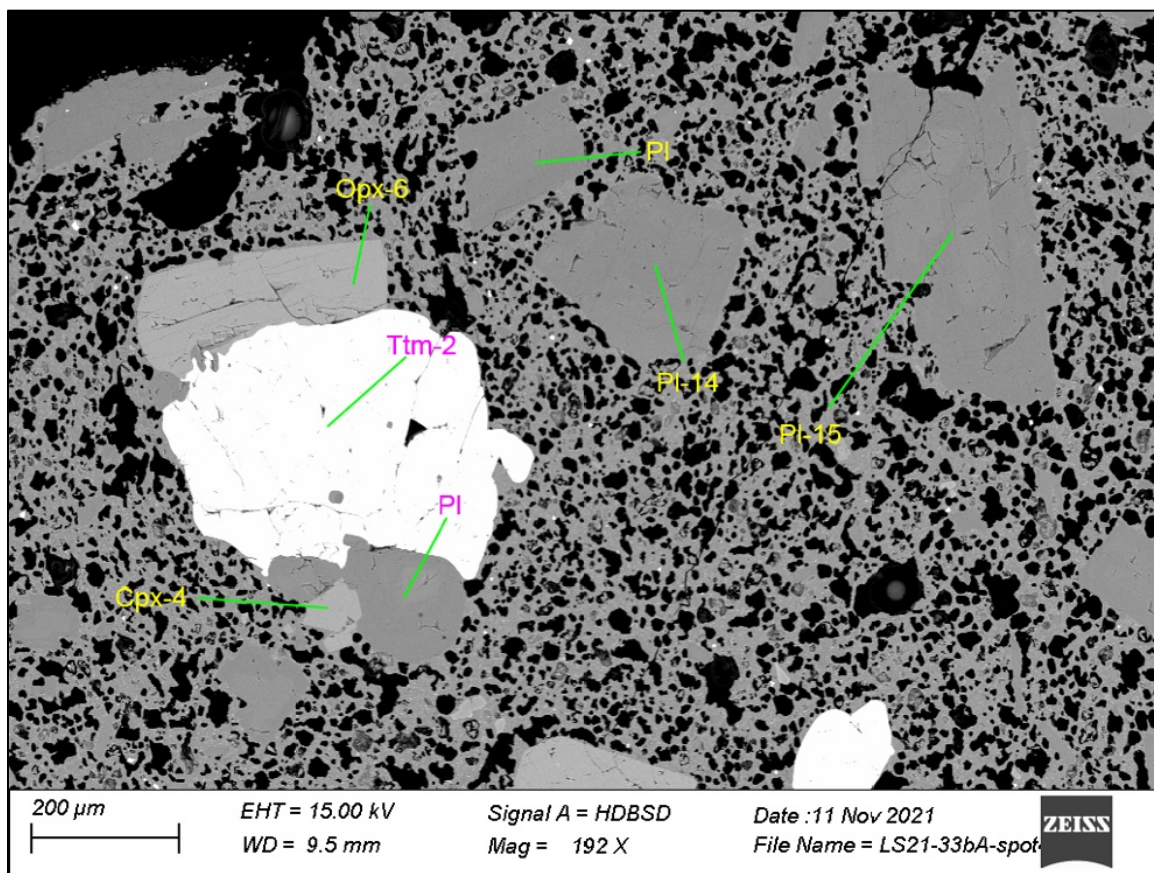


Figure 40. A BSE image of a titanomagnetite phenocryst in U1 among other mineral phases.

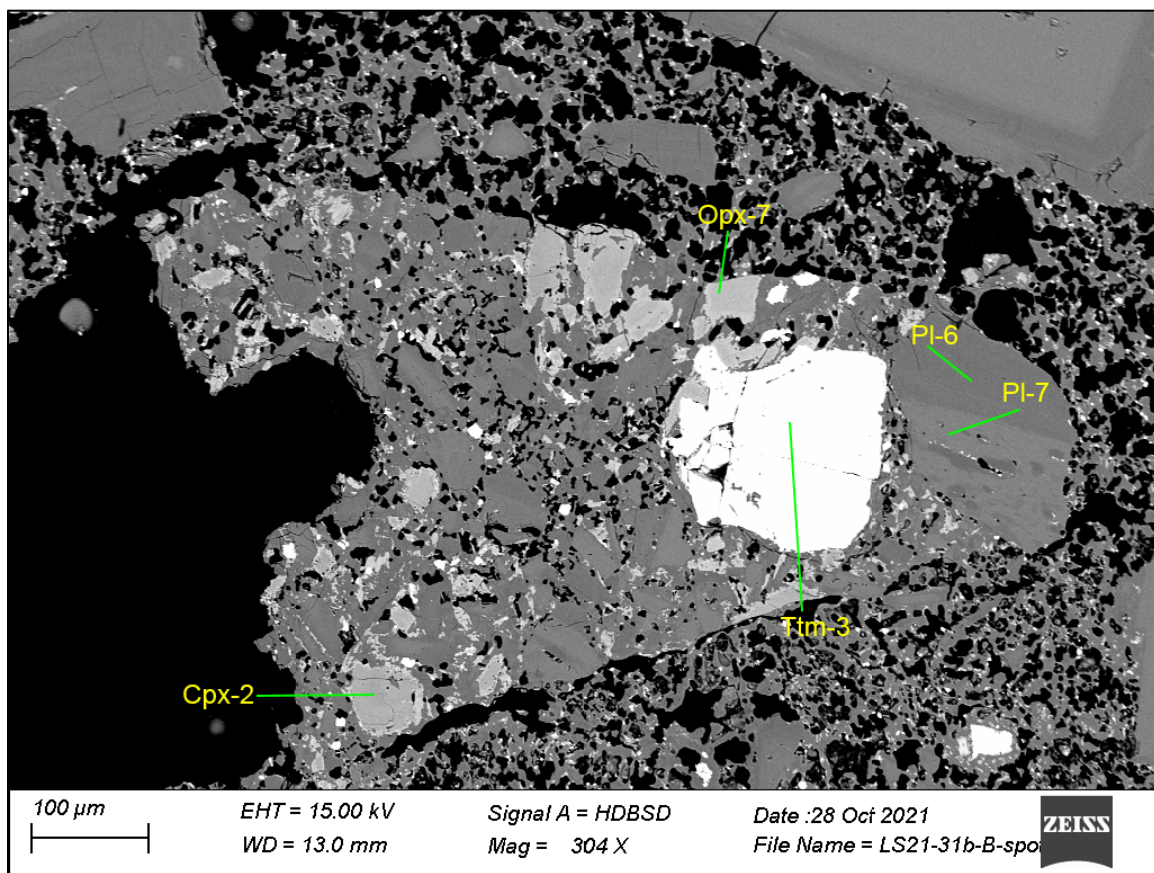


Figure 41. A BSE image of titanomagnetite phenocryst in U2 among other mineral phases in a xenocryst.

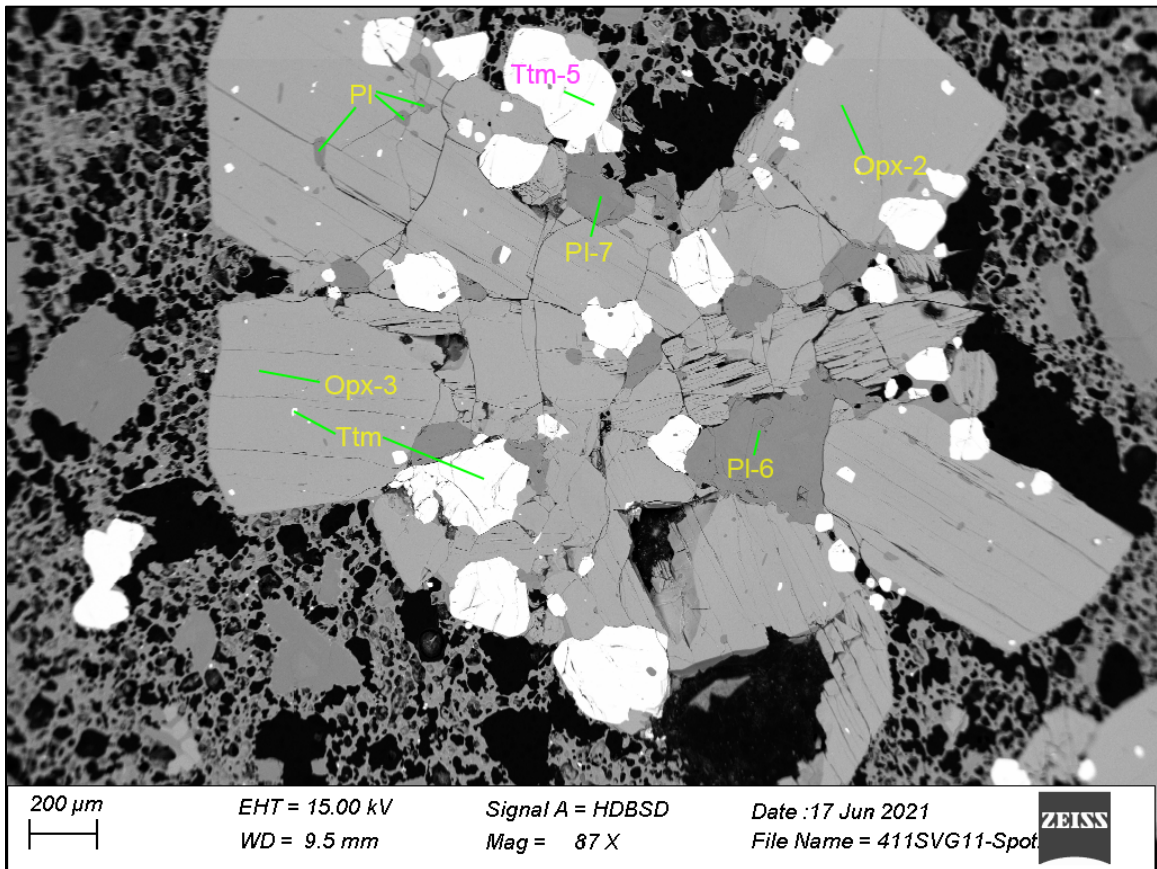


Figure 42. A BSE image of titanomagnetite phenocryst in U3 among other mineral phases in a glomerocryst.

Dome Fragments and Xenocrysts

A few distinctive clusters of minerals are present in samples from U1, U2, and U3 and appear broadly similar to glomerocrysts that are growing in the melt. However, these clasts are composed of more oxides and phosphates, such as apatite, pyrite, hematite, and/or ilmenite. Additionally, they often appear to show hydrothermal alteration or disequilibrium textures (like dissolution along crystal margins or sieve textures) (Fig. 43)

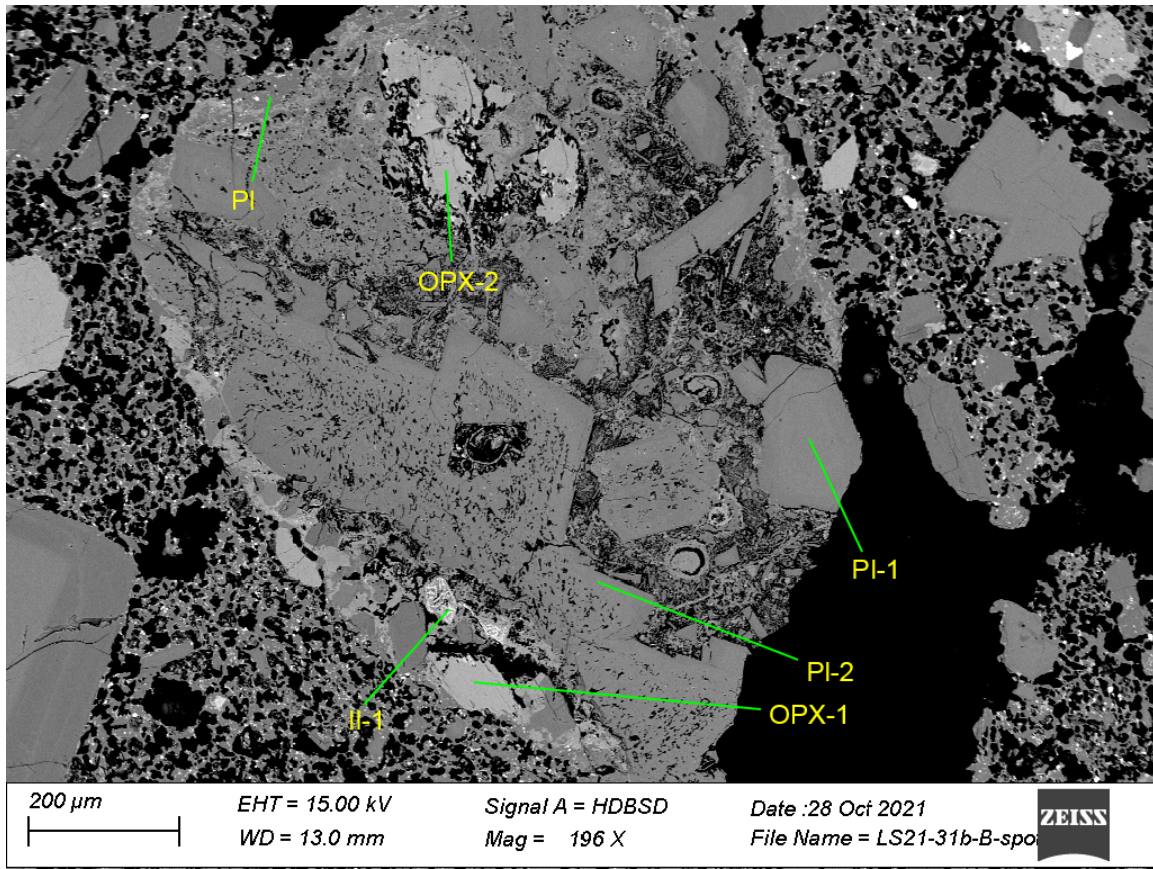


Figure 43. A BSE image of a xenocryst that includes plagioclase, orthopyroxene, and ilmenite. It also shows sieve textures throughout the different mineral phases.

Vesicle Size Distribution

The size of vesicles in samples from U1, U2, and U3 increases as the eruption progresses. Show. U1 samples are characterized by more than 60% of vesicles that are smaller than 10 μm in size (Fig. 44). U2 samples are characterized by ~43-53% of vesicles that are smaller than 10 μm in size (Fig. 45). U3 samples are characterized by less than 20% of vesicles that are smaller than 10 μm in size (Fig. 46). Collectively, this shows a distinct relationship that represents expansion and coalescence of vesicles over time.

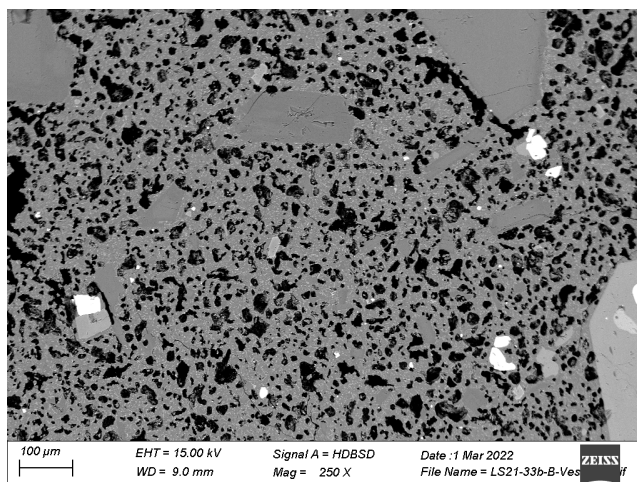


Figure 44. A BSE image of the vesicle size distribution in U1.

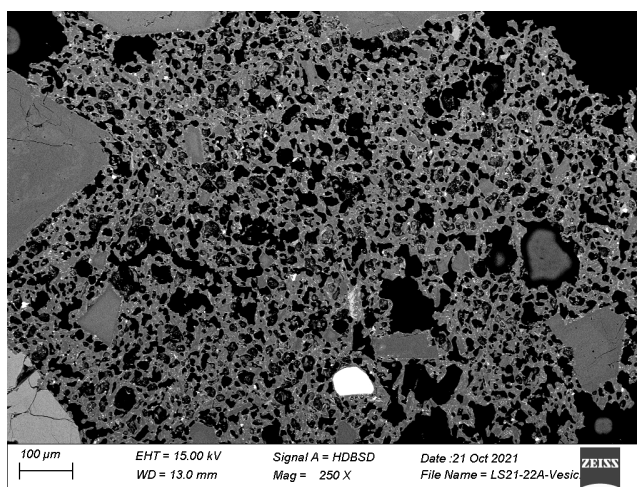


Figure 45. A BSE image of the vesicle size distribution in U2.

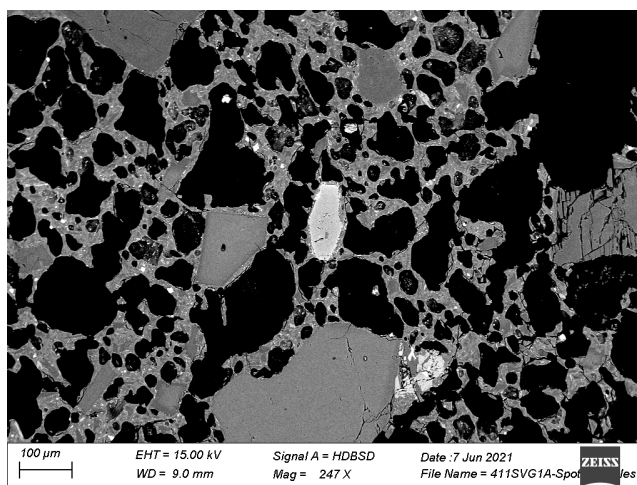


Figure 46. A BSE image of the vesicle size distribution in U3.

Gas and hydrothermal monitoring

Hydrothermal water samples were analyzed during the effusive eruption period and there was no change in elemental abundances during the dome growth phase, even just 6 days prior to the explosive eruption (Fig. 47). A slight temperature increase was noted during this period but there was no detection of degassing. Degassing was detected after the volcano transitioned to an explosive eruption style. Additionally, gas monitoring by UWI-SRC around the flanks of the volcano showed some CO₂ efflux and vegetation death, but no SO₂ was detectable during dome growth. Once the explosive began, SO₂ was readily detected by both satellites and MultiGAS.

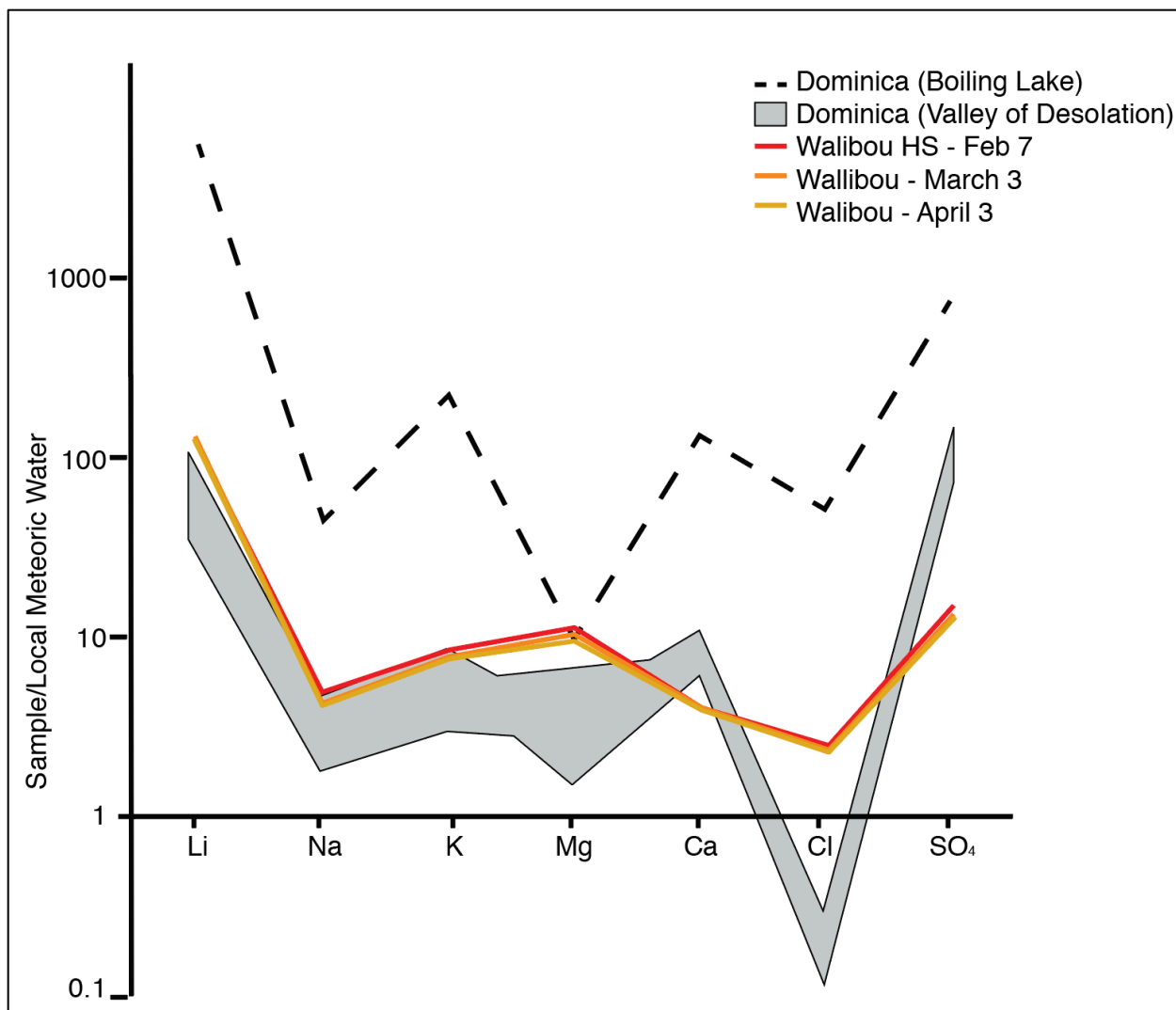


Figure 47. A chart showing the different elements present in hydrothermal water samples at the Boiling Lake and Valley of Desolation in Dominica (normalized to local meteoric water) compared to the amount present at Walibou hot springs (St. Vincent) in 2021. As depicted by the red, orange, and yellow lines, there is no change in water composition prior to the explosive eruption phases.

Discussion

Origin of Soufriere magmas – comparison of current magma to prior magmas

According to bulk rock chemistry, the scoria erupted in 2021 has a silica content that ranges ~53-57 wt%, which appears to be similar to what La Soufriere has erupted in the last 500 years (Fig. 6). La Soufriere's most common mineral assemblage remains the same as in prior eruptions, including plagioclase, clinopyroxene, orthopyroxene, olivine, and titanomagnetite. These phenocryst mineral phases are growing in equilibrium with a melt as they have euhedral edges and show no evidence of disequilibrium textures. Xenocrysts, which are very rare (only ~3-4 small fragments in 16 samples), are easily identifiable among glomerocrysts that are growing in equilibrium with the melt because they include mineral compositions, such as pyrite, apatite, and hematite, that are not found growing isolated in the melt in any thin sections (Fig. 48, 49). Mineral compositions like these are indicative of hydrothermal fluids in the magma and due to their rarity and textural disequilibrium, it is more likely that they were included from elsewhere rather than growing in the melt that produced phenocrysts.

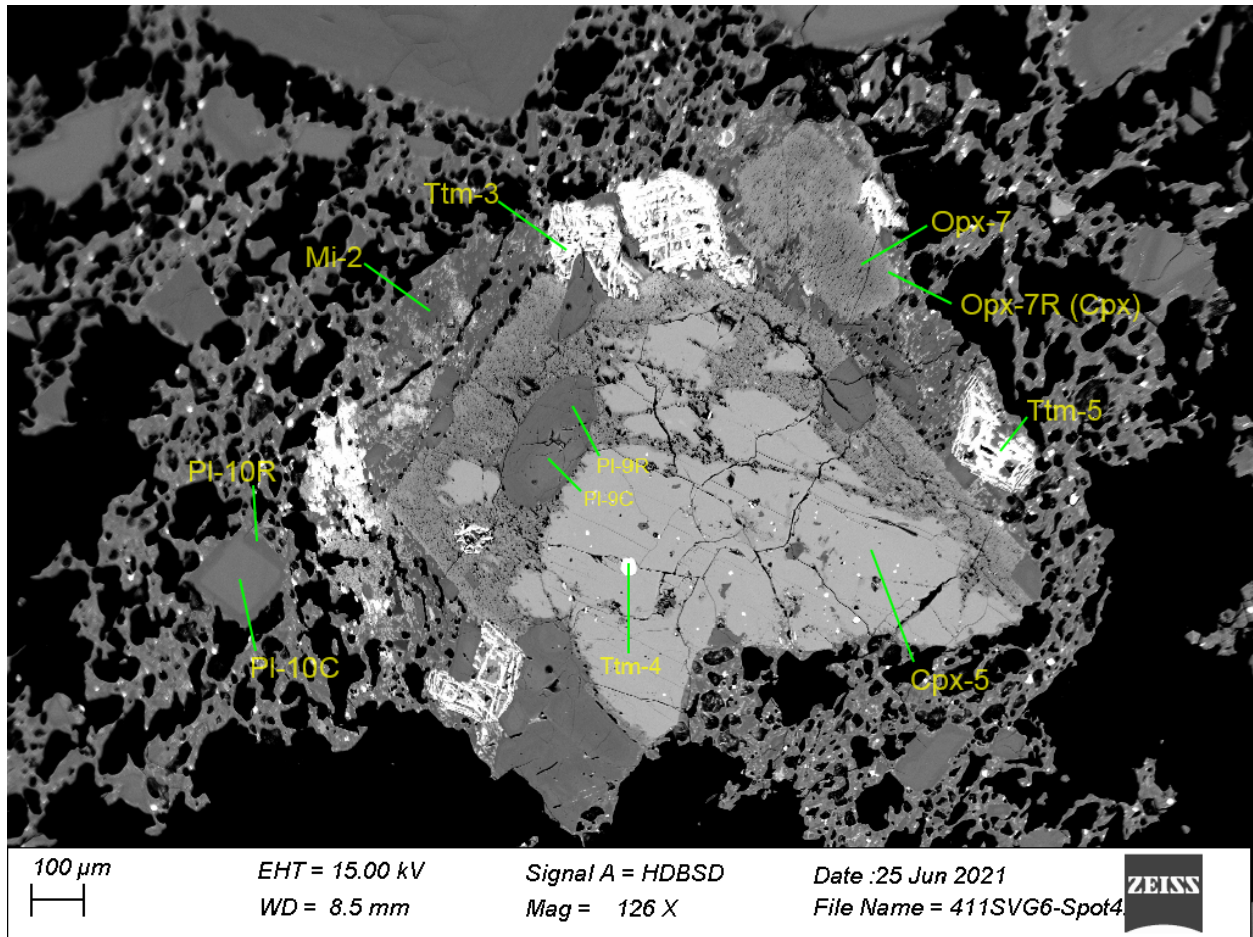


Figure 48. A BSE image of a xenocryst, or foreign rock inclusion, showing disequilibrium textures in the scoria erupted in U3. This xenocryst is likely a fragment of the pre-existing 1979 lava dome that got included in the scoria erupted in 2021, or it may be a xenocryst that was growing on the walls of the conduit and was then picked up by the magma in that erupted in 2021.

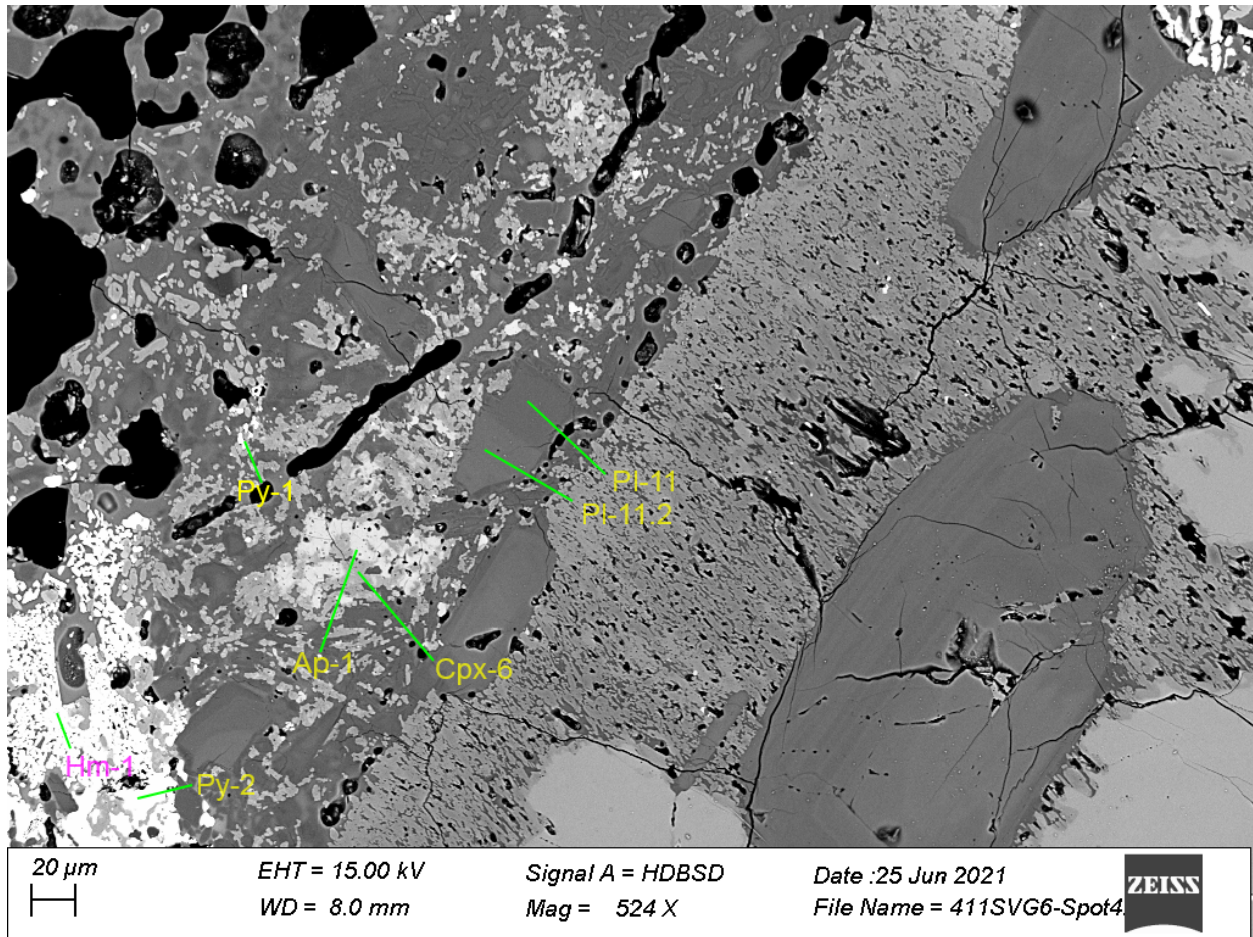


Figure 49. A BSE image (zoomed in on fig. 48) of a xenocryst that has been picked up from either the 1979 lava dome or the walls of the conduit. The image is showing a clear view of hydrothermal alteration and disequilibrium textures (sieve textures), as well as mineral compositions, like hematite, apatite, and pyrite, that do not form readily in oxidized silicic magmas. Thus, the unique mineral presence and disequilibrium textures provide direct evidence that this clast did not grow in the basaltic andesite melt and was instead included from elsewhere.

Crystal textures and compositions – introduction of magma from depth

It is clear that according to textures, the phenocrysts appear to be growing in equilibrium with a melt, however normal zoning patterns of plagioclase and clinopyroxene suggest that temperature conditions and/or the water content in the magma were not constant (Frey and Lange, 2011). Specific to normally zoned plagioclase, normally-zoned calcic cores were indicative of higher temperature crystal fractionation while the sodic rims indicated cooler temperature or lower water content conditions. This sort of change in magma chamber conditions

is common however, and results in the normal zoning patterns seen by the crystals in the scoria clasts (Lange et. al., 2009).

While microlite compositions of olivine, pyroxenes and titanomagnetites do not provide an abundance of insight into the innerworkings of the magmatic system of La Soufriere, plagioclase microlites appear to more complex than initially understood prior to recent analysis. Normally zoned plagioclase phenocrysts likely have grown in the melt over a longer period of time than microlites as they are much large in size. According to the timing of how crystals grow in the melt, however, it is expected that normally zoned plagioclase rims are going to be the last part of the crystal to grow prior to eruption. At the same time, microlites are also expected to be the last crystals to nucleate and grow upon ascent in the conduit. Thus, plagioclase microlites and plagioclase phenocryst rims should have the same chemical compositions if they are growing at the same time (Bernard and deMaisonneuve, 2020). Instead, plagioclase microlite compositions change over the course of U1, U2, and U3 becoming progressively more sodic. In U3, it is evident that plagioclase microlites are more sodic than the phenocryst rims, which suggests that the microlites and phenocrysts are not forming in the same melt. Phenocrysts likely formed in the melt over a long duration of time, perhaps multiple months, which is why they are so large, however, after analyzing the chemical equilibrium of the phenocrysts, it was concluded that the phenocrysts are not in chemical equilibrium with the melt. It is possible that something happened to the melt to change its overall composition, perhaps the introduction and mixing with a more mafic magma, after the phenocrysts had already grown (Frey and Lange, 2011). This hypothesis can be supported by looking into the FeO content and An content of the phenocrysts in comparison with the microlites (Fig. 17).

When looking into the FeO content of the phenocrysts versus the microlites, two discoveries can be made that assume that there are separate populations of microlites that are being introduced upon magma ascent, after the growth of the phenocrysts. Since phenocrysts do not form upon magma ascent in the conduit like microlites, it is assumed that they must have grown prior to the growth of any microlites (Bernard and deMaisonneuve, 2020). However, plagioclase phenocrysts have similar compositional ranges to the microlites, suggesting that they must be coming from similar depths. If the phenocrysts and microlites are forming at similar depths, it can be assumed that they likely formed at similar temperatures and similar basaltic andesite magma compositions, but ultimately formed at very different times (Bernard and deMaisonneuve, 2020).

Apart from the phenocrysts, there are two separate populations of plagioclase microlites that, according to ranges within anorthite content, are either zoned or un-zoned. Further, the iron content is distinctive within the populations of zoned and un-zoned microlites (Fig. 17). The normally zoned microlites show little variation in iron content (~ 0.6 - 0.9 wt%) in all samples, but a wide compositional range for anorthite content (~ 50 - 95 mol%). The un-zoned and Na-rich microlites show increased variability of iron content (~ 0.6 - 1.4 wt%) in all three initial explosive phases, but a more limited anorthite compositional range (~ 45 - 60 mol%).

It is important to take into account both the FeO content and the anorthite content in terms of understanding the source and timeline of growth of the plagioclase microlites in relation to the growth and source of the plagioclase phenocrysts. First, the FeO wt% in the microlites is higher than that of the phenocryst rims of the same An content, suggesting that the microlites and the phenocrysts could not have grown over the same timeline and in the same compositional body of magma. Instead, they had to have grown in separate bodies of magma that are similar in

composition, likely both basaltic andesites, but the body in which the microlites grew was more Fe-rich (Lange et. al., 2009). The differences in anorthite compositions also suggest that the calcic cored microlites formed earlier than the un-zoned microlites, in a different, more mafic (or wetter) melt, likely at greater depth. Then, upon ascent, they grew sodic rims (due to cooling of the magma) and the new, un-zoned microlites began to grow (Lange et. al., 2009).

Based on the FeO content analyses and the evidence for the two separate populations of microlites, the normally zoned and Na-rich and un-zoned microlites likely formed in two separate magma chambers, one of which was likely at a greater depth and temperature (Sisson and Grove, 1993). Since Ca is typically the first element to fractionate into plagioclase at higher temperatures, it is likely that the normally zoned microlites formed in a hotter and more mafic melt at greater depth. This melt then likely rose into the main magma chamber of La Soufriere, which is located at a higher depth and subsequently cooler temperature, resulting in more Na-rich microlites. As the Ca-rich microlites in the more mafic melt ascended into the cooler melt of the main magma chamber, it is suspected that they then grew the sodic rims, resulting in both the pre-existing Na-rich microlites and the normally zoned microlites, which have the same range in FeO. It is also suspected that even though the Ca-rich microlites came from a more mafic melt at depth, the silica content of the melt in the main magma chamber and the melt at depth were perhaps not different enough in silica composition to warrant the classic disequilibrium textures that are commonly seen in the case of a mafic injection. Instead, the more mafic melt may have only been slightly more mafic and/or hydrous, which it would be different enough to create disequilibrium and the build-up of volatiles, but not the classic disequilibrium textures since it was likely composed of the same common mineral assemblage (Melekhova et. al., 2015).

Closed to open system transition – hydrothermal gas analysis

Based on hydrothermal and gas analyses, it is likely that La Soufriere was a closed magmatic system prior to transitioning to its explosive eruptive style (Joseph et. al., 2011). Water sample analyses, however, that were conducted during the four months of effusive activity (February to early April) do not show any changes or elevated levels of hydrothermal ions (e.g. Li, SO₄) in hydrothermal waters on the island, even on April 3, which was only a few days before the volcano became explosive (Fig. 47). Therefore, it is likely that due to the lack of proper degassing, the volcano was being plugged by something, perhaps the 1979 dome and the 2020-2021 dome, resulting in a build of gases in the magmatic system (Cassidy et. al., 2018).

Closed to open system transition – vesicle nucleation and coalescence

Vesicle distributions and sizes from U1, U2, and U3 samples contribute evidence that the volcano was a closed system prior to explosivity. U1 samples were characterized by more than 60% of vesicles that were smaller than 10 µm in size (Fig. 44). The vesicles were likely smallest in this phase due to super saturation and high degree of nucleation when the magma was under the closed-system pressure prior to explosivity (Cassidy et. al., 2018). U2 samples were characterized by ~43-53% of vesicles that were smaller than 10 µm in size (Fig. 45). These vesicles were slightly larger than those in the initial phase as the initial explosion caused La Soufriere to transition from a closed to open system. Thus, once the system became open, the vesicles had more time to expand and coalesce in the conduit prior to being erupted in the second phase of explosive activity. U3 samples were characterized by less than 20% of vesicles that were smaller than 10 µm in size and the vesicles are largest in these samples due to having spent

the most time in the conduit (Fig. 46). This extended period of time allowed spent in the open-system conduit allowed them to expand and coalesce before they were erupted in the third phase of explosive activity (Blower et. al., 2001).

Conclusion

Eruptive style transitions are very common at subduction zone volcanic sites around the world and La Soufriere's eruptive history, and most recent activity, is a prime example of how quickly these transitions can occur. While no evidence of a mafic injection was found in crystal textures (e.g. reverse zone, embayments, dissolution), there were two distinct populations of microlites found throughout all three eruptive phase samples, suggesting that the zoned, Ca-rich microlites were being injected into the magma chamber from greater depth, introducing a hotter and less evolved magma into La Soufriere's system. While the magma was hotter and likely more mafic, there was not a large enough contrast between the existing magma composition and the new magma to result in a textural fingerprint. Instead, it is possible that the compositional difference was slightly lower in SiO_2 , which is why there were no disequilibrium textures evident in the scoria samples. However, the compositional difference must have been great enough to produce enough volatile build up within the closed system to result in an explosive eruption.

If the volcano had been going through a solely effusive eruption as an open system, especially during the four months of effusivity prior to explosion, there would have been noticeable CO_2 and SO_2 gas emissions and elevated Li, Br, and SO_4 signatures in water samples. Instead, all that was present was a slightly raised water temperature. This suggests that the volcano was likely plugged, creating a closed system that was not allowing for gases to be released and ultimately, a build-up in volatiles and pressure that resulted in the explosions beginning on April 9, 2021.

This case shows just how important it is to understand the inner workings of extremely active volcanic centers, especially those that are highly populated, like La Soufriere. It is

becoming increasingly more important to understand what causes effusive to explosive transitions, especially since the flanks of these volcanoes are home to thousands of people. La Soufriere, alone, has a well-known and active history of both effusive and explosive eruptions that have resulted in many deaths (e.g. 1,500 deaths in 1902) and so it is necessary to continue researching the internal mechanisms that result in eruptive transitions so that research stations and organizations, like the UWI-SRC may improve their monitoring techniques and better predict future eruptions. By combining petrology with geophysical monitoring techniques, we may better be able to predict eruptive styles and transitions in the future.

References

- Bernard, O. and de Maisonnette, C.B., 2020. Controls on eruption style at Rabaul, Papua New Guinea—insights from microlites, porosity and permeability measurements. *Journal of Volcanology and Geothermal Research*, 406, p.107068.
- Blower, J., 2001. Factors controlling permeability–porosity relationships in magma. *Bulletin of Volcanology*, 63(7), pp.497-504.
- Bouysse, P., Westercamp, D. and Andreieff, P., 1990. 4. THE LESSER ANTILLES ISLAND ARC1. In *Proceedings of the Ocean Drilling Program: Scientific results* (Vol. 110, p. 29). College Station, TX: Ocean Drilling Program.
- Cassidy, M., Manga, M., Cashman, K. and Bachmann, O., 2018. Controls on explosive-effusive volcanic eruption styles. *Nature communications*, 9(1), pp.1-16.
- Cole, P.D., Robertson, R.E.A., Fedele, L. and Scarpato, C., 2019. Explosive activity of the last 1000 years at La Soufrière, St Vincent, Lesser Antilles. *Journal of Volcanology and Geothermal Research*, 371, pp.86-100.
- Fedele, L., Cole, P.D., Scarpato, C. and Robertson, R.E., 2021. Petrological insights on the last 1000 years of explosive activity at La Soufrière volcano, St. Vincent (Lesser Antilles). *Lithos*, 392, p.106150.

Fournier, N., Moreau, M. and Robertson, R., 2011. Disappearance of a crater lake: implications for potential explosivity at Soufrière volcano, St Vincent, Lesser Antilles. *Bulletin of volcanology*, 73(5), pp.543-555.

Frey, H.M. and Lange, R.A., 2011. Phenocryst complexity in andesites and dacites from the Tequila volcanic field, Mexico: resolving the effects of degassing vs. magma mixing. *Contributions to Mineralogy and Petrology*, 162(2), pp.415-445.

Graham, A.M. and Thirlwall, M.F., 1981. Petrology of the 1979 eruption of Soufriere Volcano, St. Vincent, Lesser Antilles. *Contributions to Mineralogy and Petrology*, 76(3), pp.336-342.

Heath, E., Macdonald, R., Belkin, H., Hawkesworth, C. and Sigurdsson, H., 1998. Magmagenesis at Soufriere Volcano, St Vincent, Lesser Antilles Arc. *Journal of Petrology*, 39(10), pp.1721-1764.

Joseph, E.P., Fournier, N., Lindsay, J.M. and Fischer, T.P., 2011. Gas and water geochemistry of geothermal systems in Dominica, Lesser Antilles island arc. *Journal of volcanology and geothermal research*, 206(1-2), pp.1-14.

Lange, R.A., Frey, H.M. and Hector, J., 2009. A thermodynamic model for the plagioclase-liquid hygrometer/thermometer. *American Mineralogist*, 94(4), pp.494-506

Manon and Frey, 2022, unpublished

Melekhova, E., Blundy, J., Robertson, R. and Humphreys, M.C., 2015. Experimental evidence for polybaric differentiation of primitive arc basalt beneath St. Vincent, Lesser Antilles. *Journal of Petrology*, 56(1), pp.161-192.

Preece, K., Barclay, J., Gertisser, R. and Herd, R.A., 2013. Textural and micro-petrological variations in the eruptive products of the 2006 dome-forming eruption of Merapi volcano, Indonesia: implications for sub-surface processes. *Journal of Volcanology and Geothermal Research*, 261, pp.98-120.

Popa, R.G., Dietrich, V.J. and Bachmann, O., 2020. Effusive-explosive transitions of water-undersaturated magmas. The case study of Methana Volcano, South Aegean Arc. *Journal of Volcanology and Geothermal Research*, 399, p.106884.

Pyle, D.M., Barclay, J. and Armijos, M.T., 2018. The 1902–3 eruptions of the Soufrière, St Vincent: Impacts, relief and response. *Journal of Volcanology and Geothermal Research*, 356, pp.183-199.

Robertson, R.E.A., 2005. St. Vincent. In: Lindsay, J.M., Robertson, R.E.A., Shepherd, J.B., Ali, S. (Eds.), Volcanic Hazard Atlas of the Lesser Antilles. Seismic Research Centre, The University of the West Indies, Trinidad and Tobago, West Indies, pp. 240–261.

Sisson, T.W. and Grove, T.L., 1993. Experimental investigations of the role of H₂O in calc-alkaline differentiation and subduction zone magmatism. *Contributions to mineralogy and petrology*, 113(2), pp.143-166.

UWI-SRC FAQ